REVIEWS OF GEOPHYSICS AND SPACE PHYSICS, VOL. 11, NO. 2, PP. 427–468, MAY 1973

Kinetic Models of the Solar and Polar Winds

J. LEMAIRE AND M. SCHERER

Belgian Institute for Space Aeronomy, B-1180 Brussels, Belgium

In this paper the application of the kinetic theory to the collisionless regions of the polar and solar winds is discussed. A brief historical review is given to illustrate the evolution of the theoretical models proposed to explain the main phenomenon and observations. The parallelism between the development of the solar wind models and the evolution of the polar wind theory is stressed especially. The kinetic approaches were in both cases preceded by the hydrodynamic models, and their publication gave rise to animated controversies; later on, semikinetic and hydromagnetic approximations were introduced. A kinetic method, based on the quasi neutrality and the zero current condition in a stationary plasma with open magnetic field lines, is described. The applicability of this approach on the solar and polar winds is illustrated by comparison of the predicted results with the observations. The kinetic models are also compared with hydrodynamic ones. The validity of the criticism and remarks uttered during the Chamberlain-Parker controversy (for the solar wind), and the dispute between Banks and Holzer on the one hand, and Dessler and Cloutier on the other (for the polar wind), are carefully analyzed. The main result of this study is that both approaches are in fact not contradictory but complementary. The classical hydrodynamic descriptions are only appropriate in the collision-dominated region, whereas the kinetic theory can be applied only in the collision-free domain.

CONTENTS

A. INTRODUCTION

The polar wind, which is the escape of thermal ions out of the polar ionosphere along the open geomagnetic field lines, is a phenomenon rather similar to the well-known solar wind flow of thermal protons out of the corona.

The theoretical studies of the solar and polar winds have followed quite the same historical evolution as described in section B. Hydrodynamic models were first studied in great detail. They succeeded in giving a general representation of the number density and expansion velocity. Later on it was realized, not only that the particles in the solar and polar winds become collisionless, but also that their velocity distributions are highly anisotropic at sufficiently large radial distances. The validity of the classical theory was therefore seriously questioned and disputed. New types of descriptions more consistent with the collisionless character of these flows were then suggested to model the outermost regions. These are mainly the hydromagnetic approximations and the kinetic approaches.

The purpose of this paper is to review the application of the kinetic theory to the collision-free domains of the polar and solar winds. The general description of a kinetic theory and the basic assumptions on which it relies are given in section C. The applications to the polar and solar winds are found, respectively, in sections D and E, where the theoretical results are discussed and compared not only with other types of models but also with the observations.

B. HISTORICAL DEVELOPMENT

1. *The Solar Wind*

The purpose of this section is to recall the main steps in the development of solar wind studies, mainly of the kinetic models. Less restricted descriptions of the evolution in our understanding of the solar wind phenomenon can be found in several earlier reviews [*Parker*, 1963, 1965*a*, 1967, 1969, 1971; *Dessler*, 1967; *Ness*, 1968; *Axford*, 1968*a*; *Wilcox*, 1968; *Hundhausen*, 1968, 1970, 1972*b*; *Brandt*, 1970; *Holzer and Axford*, 1970].

a. The hydrostatic approximations. Up to 1957, the solar corona was considered a hot, fully ionized gas in hydrostatic equilibrium in the sun's gravitational field. Isothermal equilibrium was generally postulated to fit the theoretical coronal density distributions to the electron number densities observed in the near-sun region (i.e., within 10 R_S) during solar eclipses [*van de Hulst*, 1953].

In 1957, Chapman applied the theory of thermal conduction in a plasma to

make a quantitative prediction of the temperature distribution in the far outer regions of the corona [*Chapman*, 1957]. He found that the temperature should decrease in the outer regions as a consequence of the finite thermal conductivity of the hydrogen plasma. In this hydrostatic model the temperature gradient becomes superadiabatic beyond 0.22 AU, and the number density reaches a minimum value near 0.81 AU [*Chapman*, 1961]. Therefore such a static model atmosphere is convectively unstable.

b. The hydrodynamic approximations. Although much of the theoretical work on the structure of the outer corona and the interplanetary medium started with *Chapman*'s [1957] paper, the decisive step was taken by *Parker* [1958] who noted that, at large radial distances, the static models indicate a too large gas pressure. *Parker* [1958] emphasized that the coronal plasma cannot be maintained in hydrostatic equilibrium but should continuously expand into the interplanetary medium.

To have a sufficiently small gas pressure at large heliocentric distances ($r \rightarrow \infty$), the critical solution of the classical Euler hydrodynamic equations was selected to describe this steady outflow of solar plasma. In *Parker*'s [1958] isothermal corona model, the bulk velocity of the gas increases from small subsonic values in the inner corona to a highly supersonic speed at 1 AU in the interplanetary medium.

Following the same line, more elaborated hydrodynamic descriptions have been proposed to take into account the thermal conductivity [*Noble and Scarf*, 1963; *Parker*, 1964; *Whang and Chang*, 1965; *Weber*, 1970; *Cuperman and Harten*, 1970*a*; *Durney*, 1971, 1972] and the viscosity due to Coulomb collisions [*Scarf and Noble*, 1965; *Whang et al.*, 1966; *Konyukov*, 1969; *Eisler*, 1969; *Dahlberg*, 1970]. Moreover, two-fluid models and the effect of nonradial magnetic fields were also extensively examined in the hydrodynamic approximations [*Sturrock and Hartle*, 1966; *Weber and Davis*, 1967; *Hartle and Sturrock*, 1968; *Urch*, 1969; *Cuperman and Harten*, 1970*b*, 1971; *Hartle and Barnes*, 1970; *Barnes et al.*, 1971; *Whang*, 1971*a*; *Wolff et al.*, 1971].

The classical hydrodynamic equations used in this long list of papers are approximations of the general transport equations and are derived, according to the Chapman-Enskog theory, from the Boltzmann equation under the assumption that the velocity distribution of the particles is close to an isotropic and Maxwellian distribution and that the collision mean free path l is small compared with L, the smallest characteristic dimension of the system. In the first approximation (Euler) the pressure tensor is isotropic and the heat flow is zero. This corresponds to a zero mean free path approximation. In the second approximation (Navier-Stokes) the heat flow and pressure (or stress) tensors are defined to the first order in the ratio l/L in terms of the particle interaction forces. Therefore, when the ratio l/L becomes larger than 1 and the pressure tensor is highly anisotropic, these classical hydrodynamic approximations are no longer appropriate. *Hundhausen* [1968] estimated that this should occur in the solar wind beyond 0.1 AU. Although such kinds of estimations depend strongly on the adopted temperature distribution, and sometimes also on the author's personal feeling, it seems now generally accepted that the Chapman-Enskog approxi-

mation should be replaced beyond a certain heliocentric distance by some more appropriate theory. This conclusion has been anticipated by *Chamberlain* [1960], *Jensen* [1963], and *Brandt and Cassinelli* [1966], suggesting exospheric descriptions for the collisionless region of the outer corona and solar wind.

Before discussing these kinetic approaches it must be mentioned, however, that there is an equivalent way to describe a collisionless, strongly magnetized plasma on the basis of the CGL hydromagnetic equations established by *Chew et al.* [1956] and extended by *Macmahon* [1965].

c. The Chew-Goldberger-Low hydromagnetic approximations. In this CGL formulation, new expressions for the pressure tensor and heat flow are developed for collisionless plasmas under the assumption that the Larmor radius (which plays here the same role as the collision mean free path in the classical hydrodynamic theory) is small compared with the characteristic distance of the system.

In a first approximation the heat flow is assumed to be zero, as in Euler's counterpart. *Hollweg's* [1971], *Tan and Abraham-Shrauner's* [1972], and *Leer and Holzer's* [1972] applications to the collisionless solar wind are based on this first-order approximation, whereas *Whang* [1971*b*, 1972] uses a second-order approach of the CGL hydromagnetic formulation.

Although in the literature [*Holzer et al.*, 1971; *Leer and Holzer*, 1972] the CGL hydromagnetic and the classical hydrodynamic formulations are sometimes confused, they are basically different. The latter cannot describe in a fully satisfactory manner the collisionless region, and the former, which supports a comparison with the kinetic formulation, cannot correctly describe the solar wind in the collision-dominated region.

Some hybrid approximations of the transport equations with an anisotropic pressure tensor but with classical conduction and viscosity terms have also been examined [*Weber and Davis*, 1970; *Holzer and Axford*, 1970; *Leer and Axford*, 1972].

d. The kinetic approximations. Although in *van de Hulst's* [1953] review of the corona the evaporative approach and especially the work of *Pikel'ner* [1950] figure prominently, the first thoroughgoing exospheric model of the corona was given by *Chamberlain* [1960].

On the analogy of the escape of neutral particles from a planetary exosphere, Chamberlain suggested that the radial expansion of the solar corona results from the thermal evaporation of the hot coronal protons. Assuming a Pannekoek-Rosseland electric potential distribution in the ion-exosphere ($r > 2.5\ R_S$) [*Pannekoek*, 1922; *Rosseland*, 1924], Chamberlain calculated the contributions to the density, flux, bulk velocity, and average temperature of the particles moving on ballistic trajectories, with nonescaping particles moving along elliptic orbits and escaping particles moving along hyperbolic orbits. In this solar breeze model the bulk velocity remains subsonic and decreases to zero when $r \to \infty$. The pressure and density vanish also at infinity, and at 1 AU the flow speed is only 20 km sec^{-1}.

In a following paper *Chamberlain* [1961] noted that the behavior of his kinetic model is in some respects similar to that obtained by solving the hydrodynamic equations when the radial expansion is assumed to become adiabatic at

large heliocentric distances. By basing his arguments on this similarity between his evaporative and his subsonic hydrodynamic model, Chamberlain claims that Parker's 'critical' supersonic solution could not represent the steady expansion of the solar corona.

A controversy then started. *Chamberlain* [1961] argued that the supersonic solution is not supported by a physical (evaporative) model and that it results from an invalid assignment of an integration constant and an ambiguity inherent in the hydrodynamic solution. In a later note *Chamberlain* [1965] no longer disputed the likelihood that the actual solar corona is described by a supersonic solution; he merely argued for the theoretical existence of the slow solution, which at this stage was not accepted by *Parker* [1964]. Parker replied that a subsonic (adiabatic) expansion could only result in the solar corona if the temperature were larger than 4×10^6 °K [*Parker, 1965b, c*]; this would be the case if the density scale height near the sun were larger than the actual one. For a clear examination of this point we refer to *Dessler* [1967, p. 15].

Since finally the supersonic solar wind speed predicted by Parker was definitely confirmed by direct observations, Chamberlain's solar breeze model and in general any exospheric approach were considered as 'academic' solutions that might apply to very hot stars but were without any interest for the solar corona.

Even the apparently more satisfactory results obtained by *Jensen* [1963] and *Brandt and Cassinelli* [1966] did not much change this opinion. Considering a 'cones-of-escape' approach, first introduced by *Jones* [1923], and exobase levels depending on the velocity of the escaping particles, these authors obtained at 1 AU supersonic bulk velocities (290 and 266 km sec^{-1}) much larger than those in *Chamberlain's* [1960] evaporative model, which was based on a single exobase level approximation. The Pannekoek-Rosseland electrostatic potential distribution was once more adopted in these exospheric calculations. The larger supersonic expansion velocities result mainly from the fact that the calculations neglected the ballistic and satellite particle contributions to the total exosphere density.

The interest in kinetic descriptions revived, however, when *Scarf et al.* [1967] and *Hundhausen* [1968] noted that in order to explain the significantly large anisotropy of the velocity distribution observed at 1 AU, the solar wind protons should be more or less collisionless beyond a radial distance of 10 or 20 R_S. *Scarf et al.* [1967], *Hundhausen* [1968], and *Griffel and Davis* [1969], using a simple kinetic approach, calculated that the temperature anisotropy resulting from a collision-free flow of protons along a radial or a spiral interplanetary magnetic field is much larger than the observed one. Griffel and Davis concluded that there must be some relaxation mechanism (2.5 collisions/AU between 0.1 AU and 1 AU) to reduce the too large anisotropy deduced from a pure collisionless approach.

Starting also with a simple kinetic description of the solar wind protons and electrons, *Eviatar and Schulz* [1970] and *Schulz and Eviatar* [1972] came to similar conclusions and discussed some physical processes that could explain the observed proton and electron temperature anisotropies [see also *Kennel and Scarf*, 1968; *Scarf*, 1970].

At the same period *Sen* [1969], *Jockers* [1970], and *Lemaire and Scherer* [1969, 1971*b*] questioned the validity of the Pannekoek-Rosseland electric potential distribution in an ion exosphere. It is well known that such an electrostatic polarization prevents the gravitational charge separation in collision-dominated plasmas under hydrostatic equilibrium conditions. However, when the plasma density becomes so small that the charged particles escape without experiencing important deflections by the Coulomb interactions, the hydrostatic equilibrium is no longer a good approximation. The gravitational charge separation then becomes less important than the charge separation of thermal origin, and consequently the Pannekoek-Rosseland polarization field cannot be postulated. Indeed, with such an electric potential distribution, the escape flux of the electrons would be 43 times larger than the escape flux of the protons (see subsection C4).

To make these fluxes equal and to prevent a continuous charge deposition on the sun, *Sen* [1969] suggested that, by analogy with plasma sheaths in discharge tubes, some kilovolt electric potential drop should exist across the transition layer separating the collision-dominated and collision-free regions. In Sen's elementary exospheric model a proton bulk velocity of 258 km sec^{-1} is predicted at 1 AU, with an exobase at 6 R_S and a coronal temperature of 10^6 °K. Inside the ion exosphere the polarization electric field was assumed to have a Pannekoek-Rosseland type radial dependence. This assumption unfortunately does not entail the local quasi neutrality in his kinetic model.

Although in Sen's model the electric potential drop was confined in a narrow sheath at the exobase surface, it is spread out between the exobase surface and infinity in *Lemaire and Scherer*'s [1971*b*, 1972*c*] kinetic models. The value of the electric potential difference, $\phi_E(\infty) - \phi_E(r_0)$, determines the potential barrier the electrons must overcome to escape. The magnitude of this potential barrier is calculated to be such that the thermal escape flux of the electrons is reduced to a value equal to the escape flux of the protons. The local quasi neutrality condition is finally used to determine the radial distribution of $\phi_E(r)$ in the whole ion exosphere. The resulting polarization electric field is found to be quite different from the Pannekoek-Rosseland field [*Lemaire and Scherer*, 1971*b*].

Considering an exobase for the protons and the electrons at 6.6 R_S, Lemaire and Scherer's kinetic model predicts a bulk velocity ($w_E = 320$ km sec^{-1}), a density ($n_E = 7.2$ cm^{-3}), an average electron temperature ($\langle T_e \rangle_E = 1.2 \times 10^5$ °K), and an average proton temperature ($\langle T_p \rangle_E = 4.8 \times 10^4$ °K) in quite good agreement with the quiet solar wind conditions [*Hundhausen*, 1968, 1972*a*]. Too large pressure or temperature anisotropies, however, are found.

Other types of kinetic models were calculated by *Jockers* [1970], who considered an exobase at a rather low level ($r_0 = 2.5$ R_S). In his first model both the electrons and protons are assumed to be collisionless particles. In the models 2, 3, and 4, only the protons are collision free, whereas the electron gas has a fluidlike behavior, with a density determined by a barometric law and an electron temperature distribution arbitrarily specified. Henceforward we call such models semikinetic. Jocker's results show that a Parker-type supersonic expansion can

indeed be recovered with an exospheric theory. This conclusion nullified Chamberlain's argument that Parker's supersonic solution is not supported by some simple evaporative explanation. The results obtained by Jockers in his model 3 are at 1 AU: $w_E = 288$ km sec^{-1}; $n_E = 12$ cm^{-3}; $\langle T_e \rangle_E = 4.6 \times 10^5$ °K; $\langle T_p \rangle_E = 6.7 \times 10^4$ °K; and $(T_\parallel / T_\perp)_{p,E} = 900$.

With an exobase at larger heliocentric distances (10–20 R_S), *Hollweg* [1970] discussed in detail the semikinetic solutions for isothermal electron temperatures ($T_e(r) = 0.6 \times 10^6$ °K to 1.2×10^6 °K) and boundary conditions taken from *Hartle and Sturrock*'s [1968] hydrodynamic model. In his calculations the protons are assumed to become collisionless at a heliocentric distance, where they are already supersonic. The principal conclusion of this paper is that electron temperatures of the order of 10^6 °K lead to plasma flow velocities and proton temperatures that both are higher than the values obtained in the two-fluid hydrodynamic model of *Hartle and Sturrock* [1968].

In *Hollweg*'s [1970] model and in the earlier kinetic models the magnetic field was assumed to be radial or absent (which is formally equivalent). *Chen et al.* [1972] showed that the large temperature anisotropy always obtained in these kinetic models could be reduced by a factor of 5 when a more realistic spiral magnetic field is considered. This result was already anticipated by *Griffel and Davis* [1969] and was confirmed with the CGL hydromagnetic model calculations of *Hollweg* [1971] and *Leer and Holzer* [1972].

Since this reduction factor is not large enough, some additional relaxation mechanism seems to be needed to bring the temperature anisotropy of the protons in closer agreement with the observed values. Note, however, that *Tan and Abraham-Shrauner* [1972], and *Whang* [1972], using a higher-moments CGL hydromagnetic approximation, recover approximately the quiet solar wind conditions without any additional scattering or heating mechanism.

2. *The Polar Wind*

Nowadays there is no doubt that the geomagnetic field lines emerging from the polar regions are open [*Ness*, 1965] and that the ionospheric plasma, free from the restraint of the magnetic field, is not necessarily confined to the vicinity of the earth but can escape into the geomagnetic tail [*Dungey*, 1961, 1967; *Bauer*, 1966; *Dessler and Michel*, 1966; *Nishida*, 1966].

The escape energy for ions is effectively smaller than for the corresponding neutral atoms as a consequence of the polarization electric field induced in the ionosphere by gravitational charge separation. *Dessler and Michel* [1966] discussed the loss of ionized hydrogen along open field lines by means of an evaporative process similar to the evaporation of neutral hydrogen, and they estimated the number density of evaporated ionospheric plasma in the geomagnetic tail. *Bauer* [1966] described the tail of the magnetosphere as the extension of an ion exosphere and noted that the escape of ionized helium from the polar ionosphere could contribute to solving the problem of the helium budget in the terrestrial atmosphere.

Five years before, *Nicolet* [1961] had already pointed out that the thermal escape of neutral helium cannot support the large production of He^4. As the

photoionization rate of He^4 is nearly equal to its production rate, Nicolet argued that terrestrial helium should escape in its ionized state. *Axford* [1968*b*] emphasized that the helium ions are dragged away from the earth along the open magnetic field lines by the escaping photoelectrons and that the resulting flow speed can become supersonic at low altitude. In view of this, *Banks and Holzer* [1968] proposed a hydrodynamic description of this outward-flowing plasma, which, at the suggestion of *Axford* [1968*b*], was called the polar wind by analogy with the solar wind. The models they obtained by integrating the Euler equations for an isothermal temperature distribution ($T_e = T_{ion} =$ const) take into account the production of oxygen and helium ions by photoionization. The hydrogen ions result from charge transfer between O^+ and H. The electric field, which is determined by the electronic pressure gradient, is too large to hold the H^+ and He^+ ions in diffusive equilibrium, and a mass flow results. Among the infinite number of hydrodynamic solutions, *Banks and Holzer* [1968] selected the supersonic solution, which goes through the critical point, and which corresponds to a negligibly small plasma pressure at very large radial distances.

Soon after the publication of their original paper, a controversy started between *Banks and Holzer* [1969*a*] on the one hand and *Dessler and Cloutier* [1969] on the other. This debate, which recalls the earlier controversy between supporters of *Parker*'s [1958] hydrodynamic solar wind model and those of *Chamberlain*'s [1960] evaporative solar breeze solution, is discussed thoroughly by *Donahue* [1971]. The principal objection of Dessler and Cloutier concerns the pressure gradient term occurring in the hydrodynamic equations of motion. They argue that most of the acceleration of the light ions is a consequence of the charge separation electric field and that it takes place in the exosphere, where the H^+ mean free path is so long that these ions cannot be regarded as interacting directly with each other. According to Dessler and Cloutier, the acceleration of the light ions cannot be due to the partial pressure gradient. *Marubashi* [1970*a*] showed that an effective collision frequency about 10 times larger than the classical Coulomb collision frequency is required for the hydrodynamic approximation to be valid throughout the upper ionosphere. In addition to giving a very interesting description of hydrodynamic polar wind models, Marubashi discussed the possibility of an evaporative approach.

As counterpart to the hydrodynamic approach, *Dessler and Cloutier* [1969] proposed a single-particle evaporative polar breeze model in which the collisions between particles are neglected beyond some level r_0, referred to as the exobase or baropause. This exospheric level is defined as the radial distance where the mean free path of the hydrogen ions becomes equal to the scale height of the ionized oxygen. Beyond r_0 the ion acceleration is due almost entirely to the presence of the gravitationally induced electric field, which they assumed to be the well-known Pannekoek-Rosseland field in an O^+ ionosphere. *Lemaire and Scherer* [1969] showed that for such a field in the polar ion exosphere, the electron escape flux would not be equal to the total escape flux of the ions. This would lead to a continuous charge deposition in the polar ionosphere that would change the electric field in the exosphere (see subsection C4).

Lemaire and Scherer [1970, 1971*a*, 1972*a*] have considered a three-component (O^+, H^+, e) polar ionospheric model for which the charge separation electric field is determined by requiring the quasi neutrality condition and the zero electric current condition everywhere in the exosphere. Lemaire and Scherer found that the thermal electrons and oxygen ions are decelerated by the combined effect of the gravitational field and the induced electric field. The protons are accelerated outward and reach supersonic flow speeds that tend to a constant value (15–20 km sec^{-1}) at large radial distances. For the same conditions the kinetic results of Lemaire and Scherer are roughly comparable with the revised hydrodynamic calculations of Banks and Holzer [see *Mange*, 1972]. The kinetic approach, however, yielded a much more realistic oxygen ion escape flux F_{O^+} that was several orders of magnitude smaller than the O^+ flux obtained in the original hydrodynamic treatment. Although *Holzer et al.* [1971] reduced the oxygen flow in subsequent models, they still obtained too large values. In *Marubashi*'s [1970*a*] hydrodynamic model the O^+ ions are assumed to be in hydrostatic equilibrium ($F_{O^+} = 0$), which seems to be a good approximation.

By calculating collisionless polar wind models in a CGL approximation and with a semikinetic formulation, *Holzer et al.* [1971] showed that the number densities and flow speeds do not much differ in both treatments when the same boundary conditions are used at an exospheric level where the Coulomb mean free path is larger than the electron number density scale height, and where the flow speed is already supersonic. Although this agreement proves that the semikinetic formulation is nearly equivalent to the CGL hydromagnetic approximation, it does not necessarily imply the equivalence with the hydrodynamic formulation. Nevertheless, the hydrodynamic and kinetic approaches are in fact not contradictory but complementary. The hydrodynamic treatment developed by *Banks and Holzer* [1968, 1969*a*, *b*, *c*] and more recently by *Marubashi* [1970*a*] is appropriate in the collision-dominated ion barosphere, whereas the kinetic approach introduced by *Dessler and Cloutier* [1969] and modified by *Lemaire and Scherer* [1969, 1970, 1971*a*, 1972*a*] is only valid in the collision-free region of the ionosphere.

In a recent paper, *Lemaire* [1972*a*] showed how the hydrodynamic solution can be matched to the kinetic solution. Since the results of *Banks and Holzer* [1969*a*, *b*, *c*] and *Marubashi* [1970*a*] showed that the critical point of the hydrodynamic theory lies in the collision-free region, Lemaire proposed to describe the transition from a subsonic to supersonic flow by a kinetic theory. Instead of requiring that the hydrodynamic solution pass through the critical point, he chose the hydrodynamic solution that yields at the exobase a diffusion flux equal to the escape flux calculated by the kinetic method of Lemaire and Scherer.

All the models of the polar wind show that a continuous plasma escape can take place even in the winter polar ionosphere without the presence of a photoelectron flux. In the sunlit atmosphere these photoelectrons yield an additional electric drag, which is most efficient at high altitudes, where the relative abundance of the photoelectrons becomes more important. Kinetic model calculations [*Lemaire*, 1972*b*; *Lemaire and Scherer*, 1972*b*] have shown that the efflux, the

flow speed, and the parallel and perpendicular temperatures of the thermal electrons are strongly dependent on the value of the escaping photoelectron flux, whereas the number densities of the ionized hydrogen and oxygen and the thermal electrons remain practically unchanged.

Finally, it is worthwhile to mention that *Hoffman* [1968, 1970, 1971] established with Explorer 31 that at 3000 km the dominant constituent is H^+ and that O^+ is not observed at mid-latitudes and low latitudes, but that in the polar regions ionized oxygen becomes dominant as a consequence of the large efflux of ionized hydrogen streaming with supersonic velocities of 10 to 15 km sec^{-1}. Many other types of observations reviewed by *Mange* [1972] and *Marubashi* [1970*b*] show indirectly the existence of a polar wind flow.

Nevertheless, it seems that the polar wind theory has moved ahead of the available data, and therefore it is desirable to continue satellite observations of the polar upper atmosphere and particularly of the plasma flow itself.

C. THE KINETIC FORMULATION

In this chapter the approximations usually made in kinetic theories and their domain of validity are discussed (subsections C1 and C2). It is shown how the density, the flux of particles, and any higher-order moment of the velocity distribution can be calculated (subsection C3). Finally, we describe how the charge separation electric field can be determined in the collisionless region (subsection C4). The physical origin of this polarization electric field in the solar wind and in the polar wind is also discussed in the last section.

1. *The Boltzmann-Vlasov Equation*

When the binary collisions (through multiple small-angle scattering) with impact parameters smaller than the Debye length can be neglected in a low-density plasma, the Boltzmann equation can be reduced to Vlasov's equation [*Montgomery and Tidman*, 1964]

$$\frac{\partial f}{\partial t} + \mathbf{v}\cdot\frac{\partial f}{\partial \mathbf{r}} + \left[\mathbf{g} + \frac{Ze}{m}(\mathbf{E}_\parallel + \mathbf{E}_\perp + \mathbf{v}\times\mathbf{B})\right]\cdot\frac{\partial f}{\partial \mathbf{v}} = 0 \tag{1}$$

where $f(\mathbf{v}, \mathbf{r}, t)$ is the velocity distribution of the particles with mass m and charge Ze, $\mathbf{g}$ is the gravitational acceleration given by the gradient of the potential $\phi_g(r) = -GM/r$ (G is the gravitational constant and M is the mass of the central body), $\mathbf{B}$ is the magnetic field intensity, $\mathbf{E}_\perp = -\mathbf{w}_\perp \times \mathbf{B}$ is the convection electric field, and $\mathbf{w}_\perp$ is the component of the plasma bulk velocity, perpendicular to the magnetic field.

If no external electric field is applied, the small component $\mathbf{E}_\parallel$ along the magnetic field direction can be reduced to the electrostatic polarization field, preventing charge separation of gravitational or thermal origin. In the construction of Vlasov's equation, $\mathbf{E}_\parallel$ is regarded as resulting from the collective long-range interactions (or Coulomb collisions with impact parameters larger than the Debye length).

Under steady state conditions, $\mathbf{E}_\parallel$ can be derived from a potential $\phi_E(r)$,

and the Vlasov equation can be integrated immediately. The solution is given by any function of the constants of motion. If $\mathbf{v}$ and $\mathbf{v}_0$ denote the velocity of a particle at the radial distances r and r_0 along the same trajectory, the solution of Vlasov's equation is simply given by

$$f[(\mathbf{v} - \mathbf{w}_\perp)^2, \mathbf{v}_\parallel, \mathbf{r}] = f[(\mathbf{v}_0 - \mathbf{w}_{0\perp})^2, \mathbf{v}_{0\parallel}, \mathbf{r}_0] \tag{2}$$

The constants of motion are the total energy

$$W = (1/2)mv^2 + m\phi_g + Ze\phi_E = (1/2)mv_0^2 + m\phi_g(r_0) + Ze\phi_E(r_0) \tag{3}$$

and the magnetic moment

$$\mu = [(1/2)mv_\perp^2/B] = [(1/2)mv_{0\perp}^2/B_0] \tag{4}$$

under the assumption that the magnetic field intensity is strong enough to apply the guiding center approximation [*Alfvén and Fälthammar*, 1963]. For the case of a nonrotating sun or for nonconvecting geomagnetic field lines, the bulk velocity $\mathbf{w}$ is parallel to the magnetic field, and hence $w_{0\perp} = w_\perp = 0$.

2. *The Boundary Conditions*

In kinetic solar or polar wind models the velocity distribution $f(\mathbf{v}_0, \mathbf{r}_0)$ is generally specified at an exobase or baropause surface that sharply separates the collision-dominated and collisionless regions. The altitude of the exobase is determined by the condition

$$l = H \tag{5}$$

where $H = -(d \ln n_e/dr)^{-1}$ is the density scale height and l is the Coulomb deflection mean free path (mfp).

For the thermal electrons in the solar wind, l_e is given by

$$l_e = 3 \times 10^3(T_e^2/n_e) \quad \text{cm} \tag{6}$$

if $T_e = T_p$ [*Spitzer*, 1956]. For protons with a thermal speed $V_p = (3kT_p/m_p)^{1/2}$ and a bulk velocity w, the mfp is determined by

$$l_p = 7.2 \times 10^3(T_p^2/n_e)[1 + (w^2/V_p^2)]^{1/2} \quad \text{cm} \tag{7}$$

The presence of other ions or neutral atoms can reduce the mfp and therefore increase the exobase altitude.

Criterion 5 is often replaced by $\nu_{coll} = \nu_{exp}$, where ν_{coll} denotes the collision frequency and $\nu_{exp} = w|d \ln n_e/dr|$ is the expansion rate of the plasma flow. For protons with a supersonic bulk velocity ($w \gg V_p$) this second criterion is approximately equivalent to (5). Since the thermal speed of the electrons is much larger than w, however, the second criterion becomes useless for these particles [see *Jockers*, 1970, p. 228].

Actually the thickness of the transition layer between the collision-dominated and collision-free domains is of the order of the density scale height. *Jensen* [1963, Figure 7], for example, showed that the largest contribution to the escape flux of protons with a velocity nearly equal to the thermal speed ($v = (1.5)^{1/2}V_p$ and $T_p = 1.5 \times 10^6$ °K) originates in a coronal transition layer with a thickness $\Delta r_0 \simeq$

1 R_S. This layer is located at a heliocentric distance of 4 R_S where the density scale height H is approximately equal to 1 R_S [*Pottasch*, 1960], and therefore $\Delta r_0 \simeq H$. Since the extent of this layer is small compared with the extent of the collisionless region, it is usually reduced to a sharply defined surface of discontinuity beyond which the mfp becomes infinitely large. It is generally accepted that this approximation has little or no effect at distances larger than a few density scale heights above the exobase.

In kinetic models it is mostly assumed that the ion exosphere is populated by escaping particles, by ballistic particles that do not have enough energy to escape, and by trapped (or satellite) particles of which the trajectories do not cross the exobase. The velocity distribution of these trapped particles can be specified in an arbitrary way. However, if it is assumed that they are put into and removed from trapped orbits by rare collisions with the ballistic and escaping particles, it is expected that after a sufficiently long time ($\gg 1/\nu_{coll}$) their velocity distribution will be the same as that of the particles emerging from the exobase. All the incoming particles originating from the outermost regions are supposed to be missing in the collisionless region. This is artificially taken into account by a truncation of the velocity distribution $f(\mathbf{v}_0, \mathbf{r}_0)$ in certain velocity domains.

As $f(\mathbf{v}, \mathbf{r})$ and, a fortiori, its different moments are directly related to the velocity distribution at the exobase $f(\mathbf{v}_0, \mathbf{r}_0)$, it is important to determine the latter as carefully as possible. Owing to the truncation procedure that excludes the incoming particles, it is obvious that the function $f(\mathbf{v}_0, \mathbf{r}_0)$ adopted in kinetic calculations is not necessarily a realistic microscopic representation of the actual velocity distribution at the top of the collision-dominated region. It is, however, possible to build up a function of $\mathbf{v}_0$ such that the s first moments coincide with the s corresponding moments of the actual velocity distribution at r_0. Although there are many ways to build up the function, a linear combination of truncated Maxwellians

$$\sum_i c_i \exp(-\beta_i v_0^2) \tag{8}$$

is appropriate, since kinetic theories have usually been developed for Maxwellian distribution functions. The parameters c_i and β_i can be determined so that the density $n(r_0)$, the flux $F(r_0)$, the pressure tensor $\mathbf{p}(r_0)$, and any number of higher moments coincide with their actual value or some imposed value at r_0.

Although there will be no zero order discontinuity (jump) across the exobase for these specified moments, the first-order discontinuities (gradient discontinuities) cannot be avoided. This is a consequence of the sharp transition assumed between the collision-dominated and collision-free regions. From this point of view, which is not the usual one in exospheric calculations, $f(\mathbf{v}_0, \mathbf{r}_0)$ is considered an appropriate boundary value for the Vlasov equation.

In the ensuing discussion we shall consider the case where series 8 is truncated after the first term. The parameters c_1 and β_1 are determined such that $n(r_0)$ and $T_\perp(r_0)$, defined by

$$n(r_0) = c_1 \int \exp(-\beta_1 v_0^2)\, d\mathbf{v}_0 \tag{9}$$

$$T_\perp(r_0) = \frac{m}{2k} \int \exp(-\beta_1 v_0^2) v_{\perp 0}^2 \, d\mathbf{v}_0 \Big/ \int \exp(-\beta_1 v_0^2) \, d\mathbf{v}_0 \tag{10}$$

are, respectively, equal to the density and temperature at the exobase. For convenience we shall introduce two new parameters, N and T, related to c_1 and β_1 by $N = c_1(\pi/\beta_1)^{3/2}$ and $T = (m/2)k\beta_1$; i.e., the velocity distribution function at the top of the collision-dominated region is given by

$$f(\mathbf{v}_0, \mathbf{r}_0) = N(m/2\pi kT)^{3/2} \exp(-mv_0^2/2kT) \tag{11}$$

It should be noted that asymmetric Maxwellians, i.e., $\sim\exp[-\beta(\mathbf{v}_0 - \mathbf{u})^2]$, have sometimes been used instead of (11) [*Hollweg*, 1970; *Holzer et al.*, 1971; *Chen et al.*, 1972; *Lemaire and Scherer*, 1972*a*]. Moreover, kinetic formulations based on bi-Maxwellian asymmetric distributions (i.e., $\sim\exp[-\beta_\perp v_{0\perp}^2 - \beta_\parallel(\mathbf{v}_0 - \mathbf{u})_\parallel^2]$ have also been considered [*Eviatar and Schulz*, 1970; M. Scherer, unpublished data, 1971]. Although these more sophisticated approximations have their importance, they do not basically change the problem even though they complicate considerably the mathematical treatment.

3. *The Escape Flux and Higher-Order Moments of the Velocity Distribution*

The velocity distribution in the exosphere ($r > r_0$) follows immediately from (2) and (11). The density $n(r)$, the flux of particles $F(r)$, the bulk velocity $w(r) = F(r)/n(r)$, the pressure tensor components $p_\parallel(r)$ and $p_\perp(r)$, the parallel and perpendicular temperatures $T_{\parallel,\perp}(r) = p_{\parallel,\perp}/kn(r)$, and the total energy and heat fluxes $\epsilon(r)$ and $q(r)$ are directly related to the different moments of $f(\mathbf{v}, \mathbf{r})$ [*Holt and Haskell*, 1965]. They depend not only on the magnetic field configuration $\eta(r) = B(r)/B(r_0)$ and on the gravitational potential, but also on the electric potential.

The polarization electric field in the ion exosphere is of thermal origin and directed outward. Hence it is expected that the electric potential distribution $\Phi_E(r)$ will be a decreasing function of the radial distance. The potential energy of the electrons, $[m_e\Phi_g - e\Phi_E]_{r_e}^{r} = kT_eQ_e(r)$, is therefore an increasing function of r, reaching a maximum for $r \to \infty$.

The escape flux of the electrons given by

$$F_e(r) = (1/4)\eta N_e(8kT_e/\pi m_e)^{1/2}(1 + Q_e(\infty) - \Delta)\exp[-Q_e(\infty)] \tag{12}$$

is similar to the expression used by *Jeans* [1954] to calculate the efflux of neutral particles from a planetary atmosphere. The parameter Δ, entering in formula 12, is related to single φ_1 and double φ_2 layer potentials at the exobase discontinuity surface through the expression

$$\Delta = e(\varphi_1 + \varphi_2)/kT_e \tag{13}$$

Such potential jumps are often introduced in the classical electrodynamic theory at the interfaces between different electrical conductors or dielectrics [see, e.g., *Stratton*, 1941]. They can be interpreted as representing the global effects of the actual potential distribution in the transition layer separating the collision-dominated and collision-free regions. This artifice allows us to calculate the electric potential distribution in the contiguous regions without describing the detailed structure of the potential in the transition layer. Although these single-

and double-layer potentials are small and have a negligible influence at distances larger than a few scale heights from the exobase, they must be introduced in kinetic models of the solar wind to assure local quasi neutrality in the neighborhood of the exobase. In *Jockers*'s [1970] solar wind model a potential jump occurred at the exobase. Introducing a small but nonzero double-layer potential would probably have resolved the difficulties encountered by Jockers, which he describes in his Appendix 3. His electron escape flux [*Jockers*, 1970, equation A2.18] is the same as that given by (12) when $\Delta = 0$.

In kinetic models of the polar wind where the gravitationally bounded oxygen ions are predominant near the exobase, the neutralization by the electrons is easily obtained everywhere without introducing the potentials φ_1 and φ_2.

Clear evidence is given by *Jockers* [1970] that the proton total potential energy, $[m_p\phi_g + e\phi_E]_{r_e}^{r} = kT_pQ_p(r)$, reaches a maximum near 5 R_S, whereafter it decreases monotonically to a constant value at infinite radial distances. In *Lemaire and Scherer*'s [1971*b*] kinetic solar wind model, the exobase is located beyond this maximum, and $Q_p(r)$ is a negative monotonic decreasing function of the radial distance. Therefore all the protons penetrating in the ion exosphere will be accelerated outward, and the maximum proton efflux is determined by

$$F_p(r) = (1/4)\eta N_p(8kT_p/\pi m_p)^{1/2} \tag{14}$$

In the polar wind the escape flux of ionized oxygen is given by an expression similar to (12) where the subscript e should be replaced by O^+. This is because the total potential energy of the O^+ ions is an increasing function of r, since ionized oxygen is more strongly bounded by the gravitational field than accelerated by the electrostatic field. In *Holzer et al.*'s [1971] semikinetic polar wind model, the potential energy of O^+ is supposed to reach a maximum at a finite radial distance ($\simeq$13.5 R_E), beyond which it decreases to $-\infty$. In *Lemaire and Scherer*'s [1970, 1971*a*, 1972*a*] kinetic polar wind models, however, this maximum of the O^+ potential energy is only reached for $r \to \infty$. This difference is due to *Holzer et al.*'s [1971] assumption that the electrons are isothermal and distributed according to the barometric law. Indeed when this simplification is made, the electric potential is given by

$$[\Phi_E]_{r_e}^{r} = (kT_e/e) \ln [n_e/n_e(r_0)] \tag{15}$$

and since at large radial distance n_e is proportional to r^{-3}, $\lim_{r\to\infty} \phi_E(r) = -\infty$, and $\lim_{r\to\infty}$. $Q_{O^+} + (r) = -\infty$. Therefore, in Holzer et al.'s semikinetic model, the outward-directed electric force dominates the gravitational force acting on the oxygen ions beyond a radial distance of 13.5 R_E, whereas in Lemaire and Scherer's kinetic models these particles remain gravitationally bounded in the whole exosphere. This formal difference is of little practical importance, since the ionized oxygen concentration is negligibly small at these high altitudes.

The helium ions in the polar wind behave like the protons and are accelerated in the outward direction. Their escape flux is therefore given by an expression similar to (14).

The higher-order moments of the velocity distribution, yielding the density, the pressure tensor components, and the energy flux, can also be determined

analytically. For each moment there are different formulas corresponding with the two forms of the potential energy.

4. *Calculation of the Electrostatic Potential*

To determine the electrostatic potential, the local quasi neutrality condition

$$\sum_i Z_i n_i(r) = 0 \tag{16}$$

and the field-aligned electric current condition

$$\sum_i Z_i F_i(r) = F_c \tag{17}$$

can be used. For open magnetic field lines the field-aligned current or net charge flux F_c must be zero to avoid a continuous charge deposition.

As the escape fluxes $F_i(r)$ are proportional to the cross section of the magnetic field tubes, they obviously satisfy the continuity equation. Therefore it is sufficient to solve (17) at only one level, e.g., the exobase r_0. By using the analytical expressions of the fluxes in (17), it is possible to calculate by an iterative procedure the value of $\phi_E(\infty) - \phi_E(r_0)$. Finally, by using the analytical expressions of the densities, the transcendental equation (16) can be solved to determine $\phi_E(\infty) - \phi_E(r)$ at any radial distance r.

The electric potential distribution obtained with this method decreases more rapidly than the well-known Pannekoek-Rosseland potential

$$[\phi_E]_{r_0}^{r} = -\frac{\langle m \rangle_{\text{ion}} - m_e}{2e} [\phi_G]_{r_0}^{r} \tag{18}$$

where $\langle m \rangle_{\text{ion}}$ is the mean ionic mass at the distance r in the corresponding barometric model. This means that the polarization electric field accelerates the ions more strongly when the particles can escape than in the corresponding barometric case where they are in diffusive equilibrium.

In the solar wind the electric field is of thermal origin. Because the electrons have a larger tendency to penetrate and fill the collisionless region, an electric field is set up to prevent charge separation and to decelerate the electrons by transferring their thermal energy to the protons.

As suggested by *Dessler and Cloutier* [1969], this electric field is of gravitational origin in the polar wind, at least in the lower part of the ion exosphere, because in the region immediately above the exobase the gravitationally bounded O^+ ions are predominant. The resulting charge separation electric field therefore does not differ much from the Pannekoek-Rosseland field in an (O^+, e) ionosphere ($\langle m \rangle_{\text{ion}} = m_{O^+}$). Ionized hydrogen and helium are then accelerated to supersonic velocities by this large electric field [*Dessler and Cloutier*, 1969]. At higher altitudes, however, where the H^+ ions become predominant and are already supersonic, the electric field in an (O^+, H^+, e) ion exosphere decreases more rapidly than in Dessler and Cloutier's simple (O^+, e) ionosphere model [see, e.g., *Lemaire and Scherer*, 1970, Figure 6]. It is worthwhile to note, however, that the electric field decreases less rapidly than in the corresponding static (O^+, H^+, e) ionosphere model, where all the particles would be in diffusive equilibrium [see, e.g., *Lemaire*, 1972*a*, Figure 3].

Finally the charge separation that produces this electric potential can be calculated from Poisson's equation and is extremely small, as was to be expected: $\sum Z_i n_i/n_e \approx -10^{-21}$ for the solar wind, and $\approx -10^{-12}$ for the polar wind.

D. APPLICATION TO THE POLAR WIND

In this chapter the kinetic theory described above is applied to the collisionless region of the polar wind. In subsection D1 we shown how the hydrodynamic approach pertinent to the collision-dominated region can be matched to the kinetic models. The charge separation electric field distribution, discussed in subsection D2, is compared with the Pannekoek-Rosseland field as well as with the electric field distribution assumed in the polar breeze model. In subsection D3 the exospheric ion bulk velocities and densities are compared with (1) the case of diffusive equilibrium, (2) the polar breeze solution, and (3) different hydrodynamic model calculations. The comparison with the experimental results will be made in subsection D4. Finally, in subsection D5 the different theoretical formulations (kinetic, CGL hydromagnetic, and hydrodynamic) are analyzed and discussed.

1. *Baropause Conditions*

The electron density scale height and the ion mfp, which must be known to determine the baropause level by means of condition 5, can be calculated from observed density distributions in the topside polar ionosphere or from density distributions obtained by integrating upward the classical hydrodynamic equations from some low-altitude reference level.

The Ogo 2 mass spectrometer measurements in the high-altitude and high-latitude ionospheric regions provided quite accurate values for the ion number densities in the polar regions [*Taylor et al.*, 1968]. They have been used by *Lemaire* [1972*a*] to determine the boundary conditions necessary to solve the classical hydrodynamic Euler equations. For the dusk summer polar cap at an altitude of 950 km and a dip latitude of 85°, *Taylor et al.*'s [1968] observations yield $n_{O^+} = 7 \times 10^3$ cm^{-3} and $n_{H^+} = 3.2 \times 10^2$ cm^{-3}. The ion and electron temperatures in Lemaire's model are assumed to be constant and equal to 3000°K. Moreover, the neutral atmosphere model of M. Nicolet and G. Kockarts (personal communication, 1970) that corresponded to an exosphere temperature of $T_N = 1000$°K was applied to take into account the production and the interactions of ionized and neutral particles.

It is well known that the hydrodynamic solution is strongly dependent on the value of the initial bulk velocity assumed at the reference level. This value, instead of being calculated so that the hydrodynamic solution passes through the critical point, can also be determined by requiring that the diffusion flux be equal to the escape flux at the baropause [*Lemaire*, 1972*a*]. This more physical condition replaces, then, the usual critical point condition, which is a mathematical relation with little or no physical significance. Indeed, the critical point is not much more than a mathematical singularity of the Euler equations, which, for instance, does not appear in the Navier-Stokes hydrodynamic equations, when viscosity is taken into account [*Whang et al.*, 1966; *Wolff et al.*, 1971].

The results of this hydrodynamic model calculation are shown in Figures 1 and 2 by the solid lines below the horizontal bars indicating the baropause level. The bulk velocities of the ionized hydrogen (lower scale) and oxygen (upper scale) are given in Figure 1. The enhanced acceleration of the light ions in the layer just below the baropause is a consequence of the rapid decrease of the frictional force when the flow speed approaches the sonic value.

The corresponding ion number densities are shown in Figure 2 and can be compared with those of a static ionospheric model in diffusive equilibrium (dashed lines). The electron number density (not shown here) is obviously equal to the sum of the densities of ionized oxygen and hydrogen.

For the boundary conditions considered in this model the baropause altitude is $h_0 = 1250$ km. The densities and escape fluxes at this level are, respectively, $n_{O^+} = 3.61 \times 10^3\ cm^{-3}$; $n_{H^+} = 1.4 \times 10^2\ cm^{-3}$; $n_e = 3.75 \times 10^3\ cm^{-3}$; $F_{O^+} = 6.8 \times 10^{-2}\ cm^{-2}\ sec^{-1}$; $F_{H^+} = 5.44 \times 10^7\ cm^{-2}\ sec^{-1}$; and $F_e = 5.44 \times 10^7\ cm^{-2}\ sec^{-1}$.

2. *The Electric Field*

By applying the kinetic approach discussed in section C, the electric potential is determined for the boundary conditions mentioned above. The resulting parallel

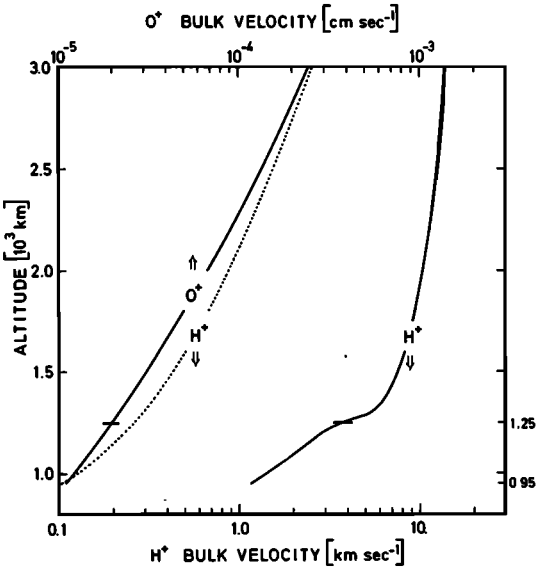

Fig. 1. The bulk velocities of the hydrogen ions (lower scale) and oxygen ions (upper scale) in the polar wind. The solid lines correspond to the kinetic model described in this paper. Below the baropause (indicated by a horizontal bar) the hydrodynamic equations are integrated for boundary conditions taken from *Taylor et al.* [1968]. The dotted line gives the H^+ ion bulk velocity of *Banks and Holzer's* [1969c] hydrodynamic model for which $T_e = T_{ion} =$ 3000°K, and $T_N = 1000$°K.

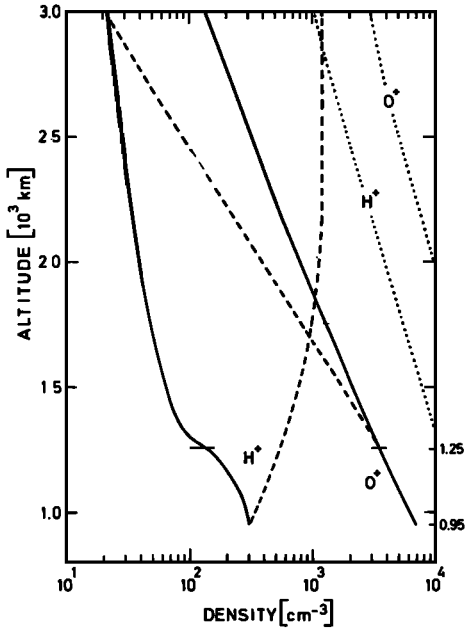

Fig. 2. The ion number densities in the polar wind. The solid lines correspond to the kinetic model described in this paper. Below the baropause (indicated by a horizontal bar) the hydrodynamic equations are integrated for boundary conditions taken from *Taylor et al.* [1968]. The dashed lines correspond to a static ionosphere in diffusive equilibrium. The dotted lines are the results of *Banks and Holzer*'s [1969*c*] hydrodynamic model for which $T_e = T_{ion} = 3000°K$, and $T_N = 1000°K$.

electric field is illustrated by the solid line in Figure 3, where the ratio of the electric force to the gravitational force acting on an oxygen ion is plotted.

In *Dessler and Cloutier*'s [1969] polar breeze model, this ratio was assumed to remain constant and equal to 0.5. It can be seen from Figure 3 that this is not too bad an approximation in the lower region where the ionized hydrogen concentration is much smaller than the oxygen ion concentration. The dashed line in Figure 3 corresponds to the Pannekoek-Rosseland field defined by (18) for a

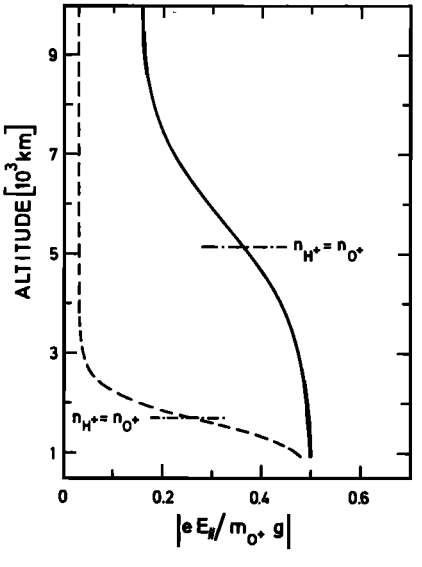

Fig. 3. The ratio of the parallel electric force to the gravitational force acting on an O^+ ion in the polar wind. The solid line corresponds to the kinetic model described in this paper. The dashed line gives the corresponding values for a static ionosphere in diffusive equilibrium. The altitude above which the H^+ ions become more abundant than the O^+ ions is also shown in both cases.

static ionosphere in diffusive equilibrium. This clearly shows that the electric force acting on the ions is larger when the particles are allowed to escape than for the case of diffusive equilibrium (see also subsection C4).

Figure 4 shows the O^+, H^+, and electron potential energies in kT units, as a function of altitude. It can be seen that the potential energies of the electrons and oxygen ions are positive increasing functions of the radial distance, and therefore the particles with an energy smaller than the potential barriers, $kT_{e(O^+)}Q_{e(O^+)}(\infty)$, will not escape. For the H^+ ions, on the contrary, $Q_{H^+}(r)$ is negative, and all the protons are therefore blown out.

Indirect evidence for the existence of the small polarization electric field (5×10^{-4} mv/m) is given at present by the outward acceleration of the light polar wind ions.

3. *Exospheric Densities and Bulk Velocities*

The bulk velocities and densities in the exosphere are given, respectively, in Figures 1 and 2 by the solid lines above the horizontal bars. It can be seen that the H^+ density decreases rapidly with altitude. Therefore the protons become the dominant constituent in the polar ionosphere only above 5000-km altitude. In the case of diffusive equilibrium (dashed lines in Figure 2) the protonosphere would start at much lower altitudes (1700 km). The O^+ density scale height is slightly larger in the polar wind than in the static model. This is a consequence of the larger electric field.

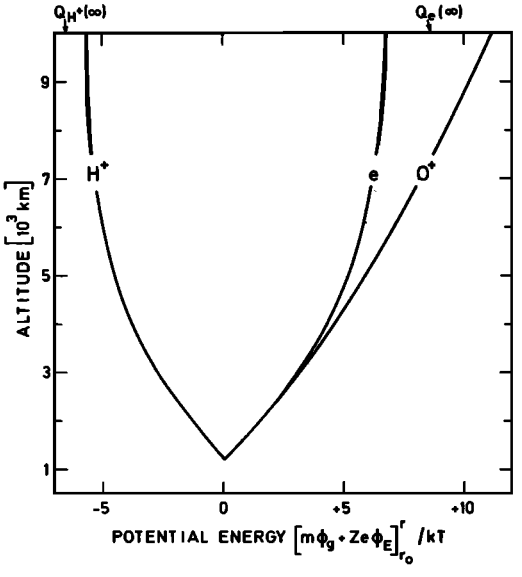

Fig. 4. The potential energy in kT units of the hydrogen ions, oxygen ions, and electrons in the kinetic polar wind model. The asymptotic values of $Q_{H^+}(h)$ and $Q_e(h)$ for $h \to \infty$ are shown by arrows; $Q_{O^+}(\infty) = +25$.

For comparison we show also the density distributions of *Banks and Holzer*'s [1969*c*] hydrodynamic polar wind model corresponding to the same temperatures ($T_{ion} = T_e = 3000°K$; $T_N = 1000°K$). The much larger ion concentrations obtained by these authors come from the fact that they used in their numerical calculations an overextended neutral atmospheric model (P. Banks, personal communication, 1972).

Figure 1 shows that, under the action of the parallel electric field, the H^+ ions acquire rapidly supersonic velocities as in *Banks and Holzer*'s [1968, 1969*b*, *c*] polar wind models. The O^+ ion bulk velocity (upper scale) increases also with altitude as a consequence of the rapid decrease of the O^+ density and the conservation of the particle efflux. Below 3000 km, the ionized oxygen bulk velocity is smaller than 3×10^{-4} cm sec^{-1}, and the oxygen ions are in near-hydrostatic equilibrium.

Banks and Holzer's [1969*c*] results for the ionized hydrogen flow speed are illustrated by a dotted line, which shows significantly smaller values than in the kinetic model. Furthermore, it must be stressed that the critical level, where the H^+ flow becomes supersonic in the hydrodynamic model, is at a rather high altitude (4000 km). This can once more be explained by the excessively large neutral atmosphere concentrations used by Banks and Holzer in their model calculations. The 10^8 times larger O^+ ion bulk velocity obtained in this hydrodynamic model (not plotted in Figure 1) is, however, much more difficult to understand.

The solid line in Figure 5 shows the hydrogen ion bulk velocity obtained by *Dessler and Cloutier* [1969] in their polar breeze model. This evaporative model calculation was based on the assumption that all the hydrogen ions have a velocity equal to the root mean square velocity ($T_{H^+} = 2000°K$) at a baropause level located at 2000-km altitude. Furthermore, in this single particle model the ions are accelerated along the magnetic field line by a charge separation electric field given by $E = -m_{O^+}g/2e$.

Banks and Holzer's [1968] first polar wind model, corresponding to an electron and ion temperature of 2000°K, is illustrated by the dotted dashed line in Figure 5 and was used by Dessler and Cloutier for comparison with the breeze solution. These polar wind bulk velocities were significantly larger than those of Dessler and Cloutier; it is probable, therefore, that they introduced the designation 'polar breeze' to contrast with the high-speed hydrodynamic solution.

However, the more recently published hydrodynamic polar wind models of *Banks and Holzer* [1969*a*, *b*, *c*] display H^+ bulk velocities that are smaller than those of the polar breeze model. The dotted line in Figure 5 corresponds to such a revised hydrodynamic model for an ion and electron temperature of 3000°K. For temperatures of 2000°K, even lower bulk velocities are expected. Therefore the controversial polar breeze has paradoxically larger flow speeds than the hydrodynamic polar wind model.

4. *Comparison with Experimental Results*

Several indirect evidences of the polar wind have been reviewed by *Banks* [1971], *Mange* [1972], and *Marubashi* [1970*b*]. Direct measurements of upward

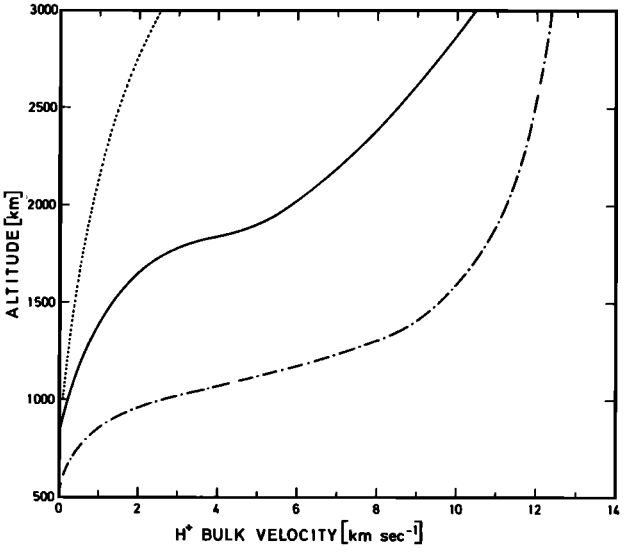

Fig. 5. The solid line corresponds to the H^+ bulk velocities calculated by *Dessler and Cloutier* [1969] in their evaporative polar breeze model (baropause altitude 2000 km, T_{H^+} = 2000°K); the dotted dashed line illustrates the H^+ flow speed obtained by *Banks and Holzer* [1968] in their first polar wind model ($T_e = T_{ion}$ = 2000°K); the dotted line gives the H^+ bulk velocity distribution published by *Banks and Holzer* [1969c] in a revised hydrodynamic model for an ion and electron temperature of 3000°K and a temperature of the neutrals T_N = 1000°K.

ionized hydrogen and helium fluxes were obtained by *Hoffman* [1968, 1970, 1971] from the Explorer 31 spacecraft. The results are summarized in the last column of Table 1 for an altitude of 3000 km in the summer polar cap region.

Column L-S in Table 1 gives for the different ionic constituents the densities n, the fluxes F, the bulk velocities w, the perpendicular temperatures $T_\perp$, the temperature anisotropies $T_\parallel/T_\perp$, and the heat fluxes q at 3000-km altitude obtained in the above-discussed kinetic model for $T_e = T_{ion}$ = 3000°K.

However, it is unlikely that the electrons and the different ion species are cooled at the same rate by collisions with the low-temperature neutral gas. Furthermore, heat conduction and the transport of energy will affect in a different way the electrons, the heavy ions, and the lighter ions. Therefore more reasonable values for the electron and ion temperatures seem to be: T_e = 4500°K; T_{H^+} = 4000°K; T_{He^+} = 3750°K; and T_{O^+} = 1500°K [*Lemaire*, 1972*a*].

The results of a kinetic calculation based on these temperatures and *Taylor et al.* [1968] ion densities at 950-km altitude (i.e., $n_{O^+} = 7 \times 10^3$ cm^{-3}; $n_{H^+} = 3.2 \times 10^2$ cm^{-3}; $n_{He^+} = 7$ cm^{-3}) are given in Table 1, column L. The densities and fluxes are of the same magnitude as *Hoffman's* [1968, 1970, 1971] summer polar cap observations. Column B-H in Table 1 corresponds to *Banks and Holzer's* [1969c] hydrodynamic model with T_N = 750°K and $T_e = T_{ion}$ = 3000°K. The

TABLE 1. Polar Wind Properties at 3000-km Altitude

Model	L-S*	L†	B-H‡	M§	Observations‖
n, cm^{-3}					
O^+	1.5×10^2	1.3×10^2	5.4×10^2	3×10^2	$0.8\text{–}2 \times 10^2$
H^+	2.1×10^1	3.6×10^1	4.4×10^2	6×10^1	$3\text{–}5 \times 10^1$
He^+		0.87	2.5		
F, cm^{-2} sec^{-1}					
O^+	3.7×10^{-2}	3.3×10^{-10}	4×10^6		
H^+	3.0×10^7	6.7×10^7	3×10^8	3×10^7	5×10^7
He^+		7.1×10^5	8×10^5		5×10^5
w, cm sec^{-1}					
O^+	2.5×10^{-4}	2.6×10^{-12}	7.8×10^3		
H^+	$14. \times 10^5$	$18. \times 10^5$	7.2×10^5	5×10^5	$10\text{–}15 \times 10^5$
He^+		8.2×10^5	3.0×10^5		
$T_\perp$, °K					
O^+	3.0×10^3	1.5×10^3	3×10^3	2×10^3	
H^+	1.5×10^3	1.8×10^3	3×10^3	2×10^3	
He^+		1.7×10^3	3×10^3		
e	2.9×10^3	4.2×10^3	3×10^3	2×10^3	
$T_\parallel/T_\perp$					
O^+	1.0000	1.0000	1	1	
H^+	0.2210	0.2079	1	1	
He^+		0.2447	1	1	
e	1.0139	1.0255	1	1	
q, erg cm^{-2} sec^{-1}					
O^+	3.2×10^{-13}	2.7×10^{-21}			
H^+	4.4×10^{-7}	1.0×10^{-6}			
He^+		1.2×10^{-8}			
e	5.2×10^{-5}	1.5×10^{-4}			

* From the present kinetic model (T_N = 1000°K, $T_e = T_{ion}$ = 3000°K).

† From *Lemaire*'s [1972*a*] model (T_N = 1000°K, T_e = 4500°K, T_{O^+} = 1500°K, T_{H^+} = 4000°K, T_{He^+} = 3750°K).

‡ From *Banks and Holzer*'s [1969*c*] model (T_N = 750°K, $T_e = T_{ion}$ = 3000°K).

§ From *Marubashi*'s [1970*a*] model (T_N = 1000°K, $T_e = T_{ion}$ = 2000°K).

‖ From *Hoffman* [1968, 1970, 1971].

results of *Marubashi*'s [1970*a*] hydrodynamic polar wind models based on *Jacchia*'s [1965] neutral atmosphere model with T_N = 1000°K, and $T_e = T_{ion}$ = 2000°K are summarized in column M of Table 1.

5. *Comparison between the Chew-Goldberger-Low Hydromagnetic Models and the Kinetic Models*

Banks and Holzer's [1968, 1969*b*] original polar wind models were based on the Euler hydrodynamic equations by analogy with the solar wind models. Later polar wind models, however, are based on CGL hydromagnetic-type equations [*Holzer et al.*, 1971]. They call this an 'extended hydrodynamic description.' Whatever the name adopted, this approach is a physically different approximation of the transport equations that is suited to describe strongly magnetized collisionless plasmas, and contrasts with the classical hydrodynamic description that should be restricted to the collision-dominated region.

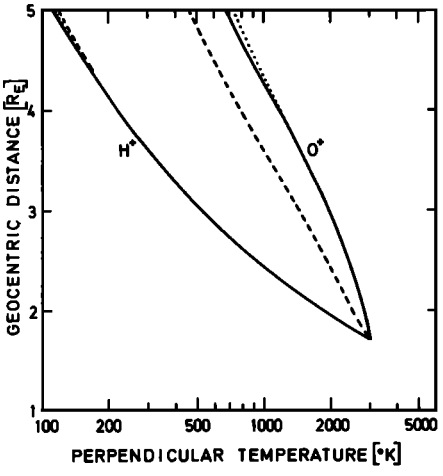

Fig. 6. The H^+ and O^+ perpendicular temperature distributions versus geocentric distance (in earth radii) for three polar wind models: the solid and dashed lines illustrate, respectively, *Holzer et al.*'s [1971] semikinetic and CGL hydromagnetic models; the dotted lines correspond to the kinetic model of J. Lemaire and M. Scherer (unpublished data, 1971) with the same boundary conditions as in the two previous cases.

Holzer et al. compared the results of this polar wind model with those of a semikinetic model. In both cases the baropause was taken at the arbitrary altitude of 4500 km, and the boundary conditions adopted at this level were taken, except for the O^+ efflux, from a hydrodynamic polar wind model of *Banks and Holzer* [1969c]. From this comparison, both descriptions give nearly equivalent results for the density, bulk velocity, and temperature profiles.

Figures 6 and 7, respectively, give the perpendicular and parallel temperature distributions of the ionized hydrogen and oxygen in the exospheric models of *Holzer et al.* [1971]. The solid lines correspond to their semikinetic calculation; the dashed lines illustrate their CGL hydromagnetic model, and the dotted lines show the results obtained in a kinetic model calculated by J. Lemaire and M. Scherer (unpublished data, 1971) with the same boundary conditions as in Holzer et al.'s models. Note that in this model the trapped orbits of the O^+ ions are supposed to be depleted as in the semikinetic model. It is easy to see

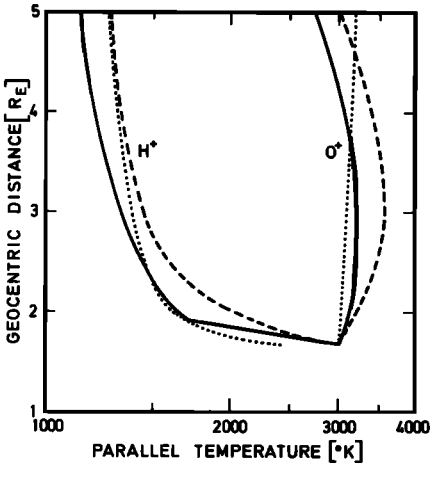

Fig. 7. The H^+ and O^+ parallel temperature distributions versus geocentric distance (in earth radii) for three polar wind models: the solid and dashed lines illustrate, respectively, *Holzer et al.*'s [1971] semikinetic and CGL hydromagnetic models; the dotted lines correspond to the kinetic model of J. Lemaire and M. Scherer (unpublished data, 1971) with the same boundary conditions as in the two previous cases.

that there is a general agreement, except for the O^+ parallel temperature. The difference is probably due to the 10^2 times larger O^+ escape flux that Holzer et al. assumed at the baropause.

It is obvious that these three sets of temperature profiles cannot, however, be compared with those obtained in a classical hydrodynamic solution, where in Euler's approximation $p_\parallel = p_\perp$ (i.e., $T_\parallel = T_\perp$), or where in the higher-order approximations of the Chapman-Enskog theory $p_\parallel \approx p_\perp$. Therefore this classical hydrodynamic treatment is inappropriate in the collisionless region. However, as noted by *Holzer et al.* [1971], this approach can provide reasonable density and bulk velocity profiles because the form of the proton pressure tensor has little effect on the flow parameters in the supersonic region. Since in the supersonic region, the pressure gradient term is small compared with the inertial term of the equation of motion, even an incorrect expression for the pressure tensor does not drastically affect the bulk velocity distribution. This feature explains why the classical or ordinary hydrodynamic equations have succeeded so well in describing the bulk velocity in the collisionless region where the flow is generally supersonic.

However, when the flow is subsonic (as for the O^+ ions), or is in the transition layer between the subsonic and supersonic regions, the pressure gradient term is not negligible in the equation of motion, and consequently the bulk velocity profile in hydrodynamic models is much more dependent on the approximation made in the definition of the pressure tensor. It is therefore hazardous to conclude from the general agreement of kinetic and CGL hydromagnetic formulations that the ordinary equations of hydrodynamics provide a good description throughout the polar ionosphere. Even if, a posteriori, the density and supersonic bulk velocity obtained with the Euler equations in the collisionless region have not unreasonable values, these classical hydrodynamic equations are useless for a more accurate description.

It has often been argued that wave particle interactions or turbulence can sometimes play the role of Coulomb collisions and maintain a fluidlike behavior above the baropause [*Koons et al.*, 1971]. In principle, this could extend the domain of application of the hydrodynamic formulation. Nevertheless, the formulation would need appropriate expressions for the pressure tensor and heat flux, taking correctly into account these non-Coulomb interactions. Since unfortunately such expressions are not available, as far as we know, the use of the classical hydrodynamic equations remains up until now limited to the barosphere.

Despite some evident limitations, the kinetic formulation has the advantage that it gives distributions of the electron and ion concentrations, bulk velocities, temperatures, heat fluxes, etc., that satisfy the collisionless transport equations exactly without solving any nonlinear differential equations. Indeed, the numerical integration of these equations is generally a very delicate matter from the technical and practical point of view. Moreover, when suprathermal particles (photoelectrons, plasma sheet, or auroral electrons and protons) have to be considered besides the thermal ionospheric ions, the kinetic theory is obviously the outsider. Applications of this type have been presented by *Lemaire and Scherer* [1972*b*, 1973].

E. APPLICATION TO THE SOLAR WIND

The solar wind conditions are certainly less favorable than the polar wind to applying a kinetic theory. Indeed, the Coulomb collisions become less rapidly negligible in the solar wind than in the polar wind. Furthermore, the ratio of the kinetic energy density to the magnetic energy density is much closer to unity in the solar wind than in the polar wind, with the consequences that the thermal plasma will more strongly influence the magnetic field structure and that plasma instabilities can also be more easily triggered.

Kinetic solar wind models describe an extreme situation where any interaction (except long-range Coulomb forces) between the particles can be completely neglected. This situation contrasts with that described by the Euler hydrodynamic model, where the collision mfp is assumed to be arbitrarily small. If a steady state quiet solar wind actually exists, it is probably something in between these two extreme models.

In subsection E1 the exobase boundary conditions are determined from a coronal density distribution observed during a solar eclipse. In subsection E2 the charge separation electric field in a kinetic solar wind model is compared with an empirical electric field distribution of the corona. The number density, the bulk velocity and proton temperatures, and the temperature anisotropies are described in subsections E3 and E4. These quantities are also compared with the quiet solar wind observations and with the results obtained in other theoretical models. In subsection E5 the correlation observed in the solar wind is compared with the positive correlation between the proton average temperatures and the bulk velocities at 1 AU, which is found by changing the exobase or coronal temperature in the kinetic models. In subsection E6 the evaporative solar breeze model is discussed and compared with the hydrodynamic solar breeze solution proposed by Chamberlain. Moreover, Parker's argument against this subsonic adiabatic solution of the coronal expansion is recalled and reinforced. The kinetic models proposed by the present authors are also compared with the hydrodynamic solutions of Parker, Durney, and Whang and Chang. Subsection E7 contains a comparison between the kinetic models and the CGL hydromagnetic models; a discussion of the validity of the classical hydrodynamic approximations is also given.

1. *Exobase Conditions*

At a sufficiently low altitude the coronal plasma is collision dominated. This is illustrated in Figure 8, where the electron mfp (dotted lines) and the proton mfp (dashed lines) are compared with the density scale height (solid lines). Curve 1 represents the density scale height from the equatorial electron number density distribution observed in the corona during the eclipse of February 1952, i.e., for a period of minimum in the sunspot cycle [*Pottasch*, 1960]. Curve 2 corresponds to the density scale height of *Hartle and Barnes*'s [1970] two-fluid solar wind model with an extra proton heating up to 22 R_S. Curves 3 and 4, respectively, show the proton and electron mfp calculated from equations 6 and 7 with the density and temperatures of Hartle and Barnes's model, which fit quite well the coronal densities observed by *Michard* [1954], *Blackwell* [1956], and

Allen [1963]. According to this model, the protons become collisionless at 8 R_S and the electrons at 20 R_S.

On the other hand, *Whang's* [1972] CGL hydromagnetic model satisfactorily represents the observed solar wind conditions near 1 AU. It has therefore been used to calculate the number density scale height (Figure 8, curve 5), the electron mfp (curve 6), and the proton mfp (curve 7) in the collisionless region. According to this model the mfp of the solar wind protons at 1 AU is 10 times larger than the density scale height H, whereas the ratio of the electron mfp to H is only equal to 2.

Figure 8 clearly shows that the solar wind can be separated into two different regions, collision-dominated and collisionless. The altitude of the common frontier of these regions depends greatly on the proton and electron temperatures.

By considering the observed coronal density distribution of *Pottasch* [1960] (curve 1 in Figure 9) and the resulting scale height (curve 2), *Lemaire and Scherer* [1971*b*] have determined the baropause altitudes h_0 as a function of the electron and proton temperatures by solving (5) with l_e and l_p, respectively, given by (6) and (7) (w was assumed to be zero in equation 7). The relationship between $T_p(h_0)$, $T_e(h_0)$, and h_0 is illustrated in Figure 9 by curves 3 and 4. For instance, if the exobase is at an altitude $h_0 = 5.6\ R_S$, then $T_e(h_0) = 1.52 \times 10^6$ °K (from curve 4), $T_p(h_0) = 0.984 \times 10^6$ °K (from curve 3), and $n(h_0) = 3.1 \times 10^4$ cm^{-3} (from curve 1). With these boundary conditions, *Lemaire and Scherer* [1971*b*, 1972*c*] calculated a kinetic model that describes rather satisfactorily the quiet solar wind density, bulk velocity, and average temperatures observed at 1 AU; this model will be used in the following description. Smaller proton or electron temperatures at the exobase would give higher exobase altitudes.

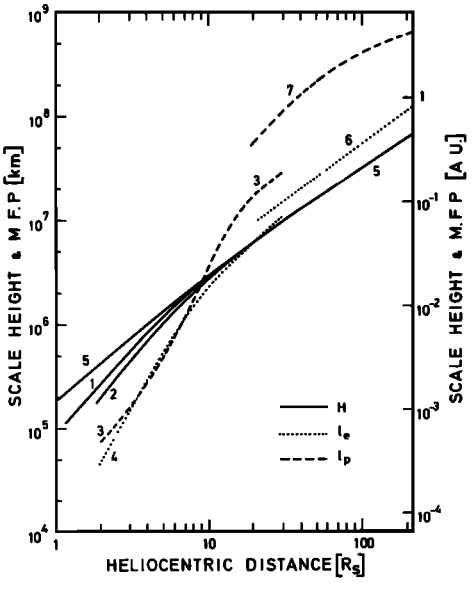

Fig. 8. The electron mfp (dotted lines), the proton mfp (dashed lines), and the density scale heights (solid lines) in the solar wind. Curve 1 shows *Pottasch's* [1960] observed coronal density distribution. Curves 2, 3, and 4 correspond to a two-fluid solar wind model of *Hartle and Barnes* [1970]. The curves 5, 6, and 7 correspond to *Whang's* [1972] CGL hydromagnetic solar wind model.

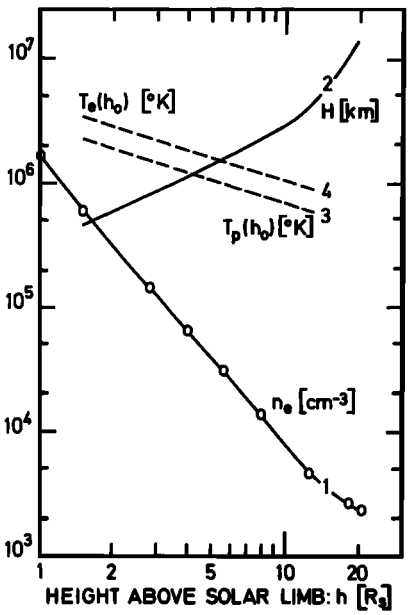

Fig. 9. Curve 1 shows the equatorial electron number density distribution per cubic centimeter in the solar corona observed during an eclipse near minimum in the sunspot cycle as reported by *Pottasch* [1960]; curve 2 gives the corresponding density scale height H in kilometers; curves 3 and 4 illustrate, respectively, the proton and electron temperatures at the exobase as a function of the exobase altitude h_0 expressed in solar radii.

2. *The Electric Field*

Solving (16) and (17), in which the electron and proton flux, respectively, are given by (12) and (14), yields the electric potential distribution in the exosphere. The values of the single- and double-layer potentials at an exobase altitude of 5.6 R_S are assumed to be $\varphi_1 = 60$ volts and $\varphi_2 = 10$ volts. The electrons and protons are supposed to become collisionless at this altitude and to move in a radial magnetic field.

The solid line in Figure 10, which illustrates the ratio of the electric force

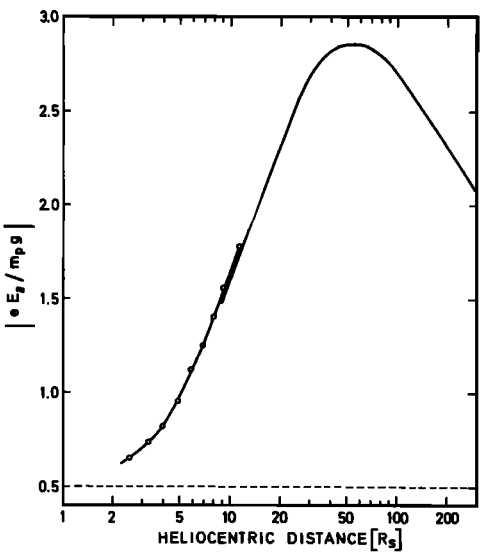

Fig. 10. The ratio of the parallel electric force to the gravitational force acting on a proton in the solar wind. The solid line corresponds to the kinetic model 1 of *Lemaire and Scherer* [1972c]. The dots correspond to empirical values deduced from *Pottasch*'s [1960] observed coronal density distribution. The dashed line corresponds to Pannekoek-Rosseland's electrostatic potential distribution.

to the gravitational force acting on a proton, is in this kinetic model quite different from the Pannekoek-Rosseland potential, for which this ratio is constant and equal to 0.5 (see dashed line).

An empirical electric field distribution (open dots in Figure 10) can also be obtained from *Pottasch*'s [1960] observed density and scale height distributions illustrated by curves 1 and 2 in Figure 9 [*Lemaire and Scherer*, 1971*b*; see also *Sen*, 1969]. Indeed, assuming a constant electron temperature, $T_e = 1.52 \times 10^6$ °K, the electric field in the corona is given by

$$\frac{eE_\parallel}{m_p g} = -\frac{kT_e}{m_p g}\frac{\nabla n_e}{n_e} = \frac{kT_e}{m_p g}\frac{1}{H(r)} \tag{19}$$

In the overlapping region the agreement between this empirically determined electric field distribution and that of the kinetic model is excellent and seems to indicate that the electron temperature gradient (assumed to be zero in equation 19) is indeed not very important in the region between 6 and 20 R_S.

At 1 AU, the parallel electric field intensity is 10^{-10} v/m, which is much smaller than the convection electric field $\mathbf{E}_\perp = -\mathbf{w}_\perp \times \mathbf{B}$ (10^{-6} v/m). The polarization electric field is, however, two orders of magnitude larger than the 'runaway' field at 1 AU [*Scarf*, 1970]. It is therefore reasonable to expect that small fluctuations in the value of the parallel electric field can provide drift currents large enough to trigger two-stream instabilities and to produce ion acoustic radiation at 1 AU and even in the whole collisionless region.

3. *The Density and Flow Speed*

The solid line in Figure 11*a* shows the density distribution in the kinetic model. The asymptotic behavior, as $r \to \infty$, is shown by the dashed line [*Lemaire and Scherer*, 1972*c*]. The squares in the left-hand side are *Pottasch*'s [1960] observed coronal densities. They are in good agreement with the theoretical values. Note the absence of a discontinuity at the exobase, which is often seen in earlier exospheric models (see subsection C2).

Figure 11*b* shows the bulk velocity distribution (solid line) with its asymptotic value (dashed line). The solar wind velocity, as well as the density at 1 AU, is not in disagreement with the range of observed values shown by vertical bars.

The first line in Table 2 summarizes the observed quiet solar wind conditions given by *Hundhausen et al.* [1970] and *Hundhausen* [1972*a*, *b*]. The second line shows the results obtained at 1 AU in the present kinetic model, which corresponds also to *Lemaire and Scherer*'s [1972*c*] model 1. The third line refers to a similar kinetic model with an asymmetric proton velocity distribution at the exobase, i.e.,

$$f_p(\mathbf{v}_0, \mathbf{r}_0) = c_p \exp\left[-\beta_p(\mathbf{v}_0 - \mathbf{u}_0)^2\right] \tag{20}$$

for which $u_0 = 14$ km sec^{-1} is a best fit value to recover the observed quiet solar wind average proton temperature at 1 AU [*Lemaire and Scherer*, 1971*b*]. The fourth line corresponds to *Jockers*'s [1970] semikinetic model 3, for an exobase at $r_0 = 2.5\ R_S$ and an arbitrary electron temperature distribution: $T_e(r) = 1.32 \times 10^6$ °K for $r < 9\ R_S$, and $T_e(r) \sim r^{-1/3}$ for $r > 9\ R_S$. The fifth line gives

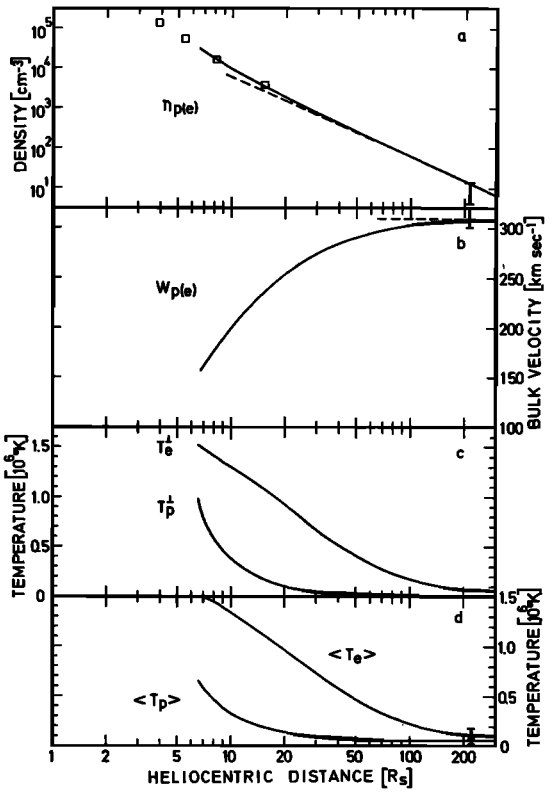

Fig. 11. The solid lines give (*a*) the density, (*b*) bulk velocity, (*c*) perpendicular temperature, and (*d*) average temperature of the electrons and protons in *Lemaire and Scherer*'s [1972*c*] kinetic model 1. The asymptotic behaviors are illustrated by dashed lines. The observed coronal density distribution reported by *Pottasch* [1960] is shown by squares. The range of observed solar wind properties at 1 AU are taken from *Hundhausen et al.* [1970] and are indicated by vertical bars.

the results of *Hollweg*'s [1970] semikinetic model, calculated for a highly asymmetric proton velocity distribution (equation 20 with $u_0 = 200$ km sec^{-1}) at the exobase level $r_0 = 20\ R_S$. The sixth line refers to *Chen et al.*'s [1972] semikinetic model with the same exobase boundary conditions as in Hollweg's calculations but with a spiral magnetic field and a polytropic electron temperature distribution. The results of the kinetic models of *Chamberlain* [1960], *Jensen* [1963], *Brandt and Cassinelli* [1966], and *Sen* [1969] are given in the last four lines of Table 2.

4. *Temperature Distributions*

In Figures 11*c*, *d* the radial distributions of the perpendicular and average temperatures of the electrons and protons are displayed. The average tempera-

TABLE 2. Solar Wind Properties at 1 AU

Models	w, km sec^{-1}	n, cm^{-3}	$\langle T_e \rangle$, 10^4 °K	$\langle T_p \rangle$, 10^4 °K	$T_{e\parallel}/T_{e\perp}$	$T_{p\parallel}/T_{p\perp}$
1	300–350	8.7 ± 4.6	14 ± 5	4.4 ± 1.8	1.1–1.2	2.0 ± 1
2	307	12.9	11.5	4.49	3.04	160
3	320	7.2	11.7	4.8	3.05	164
4	288	12	46	6.7	1.00	900
5	330		100	0.9	1.00	45
6	313		60	0.41	1.00	11
7	20	370		11		
8	290	2.7				
9	266	3.2		12		
10	258	3.34				

Model 1, the observed quiet solar wind conditions [*Hundhausen et al.*, 1970; *Hundhausen*, 1972*a*].

Model 2, from the present kinetic model (see also *Lemaire and Scherer* [1972*c*]).

Model 3, from *Lemaire and Scherer*'s [1971*b*] kinetic model with an asymmetric velocity distribution.

Model 4, from *Jockers*'s [1970] semikinetic model 3.

Model 5, from *Hollweg*'s [1970] semikinetic model with $T_e(r) = 10^6$ °K.

Model 6, from *Chen et al.*'s [1972] semikinetic model with a spiral magnetic field and a polytropic electron temperature distribution.

Model 7, from *Chamberlain*'s [1960] evaporative breeze model.

Model 8, from *Jensen*'s [1963] exospheric model.

Model 9, from *Brandt and Cassinelli*'s [1966] exospheric model.

Model 10, from *Sen*'s [1969] kinetic model.

tures, $\langle T \rangle = \frac{1}{3} (T_\parallel + 2\, T_\perp)$, and the temperature anisotropies at 1 AU are also reported in Table 2 (line 2), where they can be compared with the observed values (line 1) or with other kinetic and semikinetic model results.

It appears that when the exobase conditions are not arbitrarily chosen but are deduced from an observed coronal density distribution, the predicted average electron and proton temperatures are consistent with the observations at 1 AU. The low proton temperatures obtained by *Hollweg* [1970] and the even lower values calculated by *Chen et al.* [1972] when a spiral magnetic field is taken into account are probably due to the rather low exobase proton temperature 7×10^4 °K assumed by these authors. By using boundary conditions similar to those of *Hollweg* [1970] at an exobase of 20 R_S, our kinetic model calculations yield $\langle T_p \rangle = 1.2 \times 10^4$ °K; $T_{p\parallel}/T_{p\perp} = 60$; and $w = 280$ km sec^{-1} at 1 AU.

Kinetic models predict generally larger parallel than perpendicular temperatures, which is in compliance with the observations. The ratio $T_\parallel/T_\perp$, however, is extremely large and unrealistic. This feature, which is probably the strongest limitation of kinetic models for the solar wind, has been noted earlier by *Scarf et al.* [1967], *Hundhausen* [1968], and *Griffel and Davis* [1969].

Chen et al. [1972] have shown that if a spiral interplanetary magnetic field is introduced, this anisotropy could be reduced by a factor of 5. This geometrical reduction is nevertheless still too small to bring the proton temperature anisotropy into the range of the observed values at 1 AU.

The relatively smaller temperature anisotropy of the electrons in our models ($T_{e\parallel}/T_{e\perp} \approx 3$) is a consequence of the large number of trapped electrons as compared with the number of escaping electrons present at 1 AU. This anisotropy is also too large, according to the observations, and leads to the suggestion that some scattering mechanism besides the rare Coulomb collisions must modify the pitch angle distribution of the charged particles between the exobase and 1 AU. This presumed mechanism must not be too strong to avoid $T_\parallel/T_\perp$ becoming equal to 1. Nevertheless, it has to be strong enough to reduce the proton and electron temperature anisotropies of pure collisionless models by factors larger than 10 and 2, respectively. An effective proton collision rate of 2.5 collisions/AU was suggested by *Griffel and Davis* [1969]. Moreover, this additional process should not significantly change the kinetic energy of the protons and electrons, because the average temperatures obtained with the collision-free hypothesis are in satisfactory agreement with the observations [see also *Whang*, 1972].

Different types of wave particle interactions have been suggested to scatter the particles in the collisionless solar wind region [*Scarf et al.*, 1967; *Kennel and Scarf*, 1968; *Forslund*, 1970; *Eviatar and Schulz*, 1970; *Schulz and Eviatar*, 1972; *Hollweg and Völk*, 1970]. For an extensive review we refer to *Scarf* [1970].

I. Axford (personal communication, 1970) suggested that Coulomb collisions, despite their low rate, could contribute to maintaining the temperature anisotropies close to the observed values. Indeed, because the time constant for equipartition of energy between the electron gas and the proton gas is about 43 times larger than the proton collision time for angular deflections, the particle-particle interactions will mainly scatter the particles without transferring energy from one kind of particles to the other, i.e., without changing $\langle T_e \rangle$ and $\langle T_p \rangle$. However, no definitive indication can be given at this time for deciding which among all these scattering mechanisms is (or are) the most effective in the collisionless solar wind region.

5. *Correlations in the Solar Wind*

To obtain a good representation of the quiet solar wind conditions, the baropause was taken at an altitude of 5.6 R_S. It is possible, however, to generate a whole set of kinetic models with baropause altitudes ranging from 2 R_S to 13 R_S. In each of these models the boundary conditions can be determined from curves 1, 2, and 3 in Figure 9. In this case the exobase density and the proton and electron temperatures range, respectively, from 3.1×10^5 to 4.3×10^3 cm^{-3}, from 1.8×10^6 to 0.58×10^6 °K, and from 2.8×10^6 to 0.9×10^6 °K. The bulk velocity w_E and the average proton temperature $\langle T_p \rangle_E$ at 1 AU can be calculated for these sets of exobase conditions. These results can be plotted in the $(w_E, \langle T_p \rangle_E)$ plane and are represented by the solid line in Figure 12, taken from *Lemaire* [1971].

It is found that any increase of the coronal temperatures, $T_p(h_0)$ and $T_e(h_0)$, corresponding to a decrease of the exobase altitude, results in an increased solar wind average proton temperature and bulk velocity but does not much affect the average electron temperature at 1 AU [*Lemaire and Scherer*, 1971*b*]. This absence of correlation between the average electron temperature and w_E is in

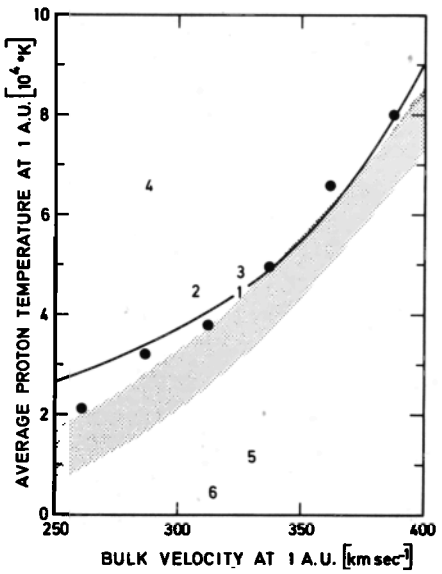

Fig. 12. Correlation between the solar wind velocities and average proton temperatures at 1 AU. The solid dots correspond to Vela 3 measurements [*Hundhausen et al.*, 1970]. The shaded area corresponds to Explorer 34 data illustrated by the relation $\langle T_p \rangle_E = (0.036 \pm 0.003) w_E - (5.54 \pm 1.50)$ proposed by *Burlaga and Ogilvie* [1970]. Point 1 gives the quiet solar wind condition [*Hundhausen*, 1972*a*]; points 2–6 give the results obtained from the kinetic and semikinetic models reported in Table 2 from the second to the sixth line. The solid line shows the relationship deduced by *Lemaire* [1971] and discussed in the text.

agreement with the solar wind observations of *Montgomery et al.* [1968] and *Serbu* [1972] and is also discussed by *Burlaga and Ogilvie* [1970].

The positive correlation between $\langle T_p \rangle_E$ and w_E shown by the solid line in Figure 12 agrees well with the results obtained by *Hundhausen et al.* [1970] from Vela 3 measurements (solid dots) and by *Burlaga and Ogilvie* [1970] from Explorer 34 data (shaded area). The points 1–6 correspond to the quiet solar wind conditions and to the kinetic or semikinetic models reported in Table 2.

Hartle and Barnes [1970] have shown that a similar positive correlation between $\langle T_p \rangle_E$ and w_E can also be deduced from a continuous set of two-fluid hydrodynamic models with an extra heating of the protons in a region extending up to 25 R_S in the corona. When the amplitude of the heat source is increased, Hartle and Barnes found that the proton temperature and bulk velocity are both increased. The observed correlation can then be reproduced by choosing correctly the intensity of the heat source [*Barnes et al.*, 1971]. As the coronal temperature $T_p(h_0)$ is directly related to the heat deposition in the collision-dominated region, this conclusion of Hartle and Barnes supports also the results obtained by *Lemaire and Scherer* [1971*b*] that larger values of w_E and $\langle T_p \rangle_E$ follow from an increase of the exobase temperatures.

As suggested by *Lemaire* [1971], the slight deviations of the predicted $(w_E, \langle T_p \rangle_E)$ relationship from the observed relationship for $w_E < 300$ km sec^{-1} and $w_E > 370$ km sec^{-1} are probably consequences of the assumption that *Pottasch*'s [1960] mean coronal densities (Figure 9, curve 1) correspond as well to hot as to colder coronal temperatures. If, however, the corona and the solar wind are considered as a collection of hot and cold streamers, the density distributions inside these streamers will depart from this observed mean distribution. Consequently, the exobase corresponding to large (or small) values of $T_e(h_0)$

will be at higher (or lower) altitudes than those predicted in Figure 9. These corrections can bring the solid curve of Figure 12 in closer agreement with the observations for $w_E < 300$ km sec^{-1} and $w_E > 370$ km sec^{-1}.

Lemaire [1971] has shown that the same adjustment gives also a closer fit for the (n_E, w_E) relationship determined theoretically from *Lemaire and Scherer*'s [1971*b*] kinetic calculation and experimentally from *Hundhausen et al.*'s [1970] observations.

It should also be noted that the electron heat or 'conduction' flow at 1 AU is positively correlated with w_E and that it is of the same order of magnitude as *Montgomery et al.*'s [1968] estimation from the Vela 4 measurements [*Hundhausen*, 1970].

6. *Kinetic versus Hydrodynamic Models*

A first comparison between kinetic and hydrodynamic solar wind models was made by *Chamberlain* [1960, 1961]. The solar breeze model of *Chamberlain* [1960] was based on the following assumptions: (1) above an exobase level the particles can move collision free on ballistic, satellite, and hyperbolic trajectories with no particles coming from infinity; (2) besides the gravitational potential ϕ_g, there is a polarization electric potential ϕ_E given by the Pannekoek-Rosseland formula (18). For proton and electron number densities and temperatures, respectively, given by $n(r_0) = 10^6$ cm^{-3} and $T(r_0) = 2 \times 10^6$ °K at an exobase $r_0 = 2.5\ R_S$, Chamberlain obtained the rather high density and small bulk velocity reported in Table 2 (line 7).

This solar breeze model and any other kinetic model satisfy the general collisionless transport equations. Under the assumption of steady state conditions and radial symmetry, these equations become

$$nwr^2 = C \tag{21}$$

$$nmw\frac{dw}{dr} + \frac{d}{dr}(nkT_\parallel) + \frac{2nk}{r}(T_\parallel - T_\perp) = -nm\frac{d}{dr}\phi_g - Zen\frac{d}{dr}\phi_E \tag{22}$$

$$r^2q + C\left[\frac{1}{2}mw^2 + \frac{k}{2}(3T_\parallel + 2T_\perp) + m\phi_g + Ze\phi_E\right] = E_\infty \tag{23}$$

where $4\pi C$ and $4\pi E_\infty$ are, respectively, the total particle flux and energy flux. The five terms in the left-hand side of (23) represent, from the left to the right, (1) the heat or conduction flux, (2) the convection of kinetic energy, (3) enthalpy, (4) gravitational energy, and (5) electrostatic energy. A similar set of equations can be written for the collisionless protons and for the collisionless electrons; for convenience the subscripts p and e have been omitted in (21–23).

Taking into account the quasi neutrality condition (16), equations 21–23 applied to the electrons can be added to the corresponding set of equations for the protons. This eliminates the electric potential ϕ_E in the equation of motion (22) and in the equation of energy (23).

In *Chamberlain*'s [1960] evaporative solar breeze solution, the asymptotic

behaviors for $r \to \infty$ are given by $w \sim r^{-1/2}$; $n \sim r^{-3/2}$; $T_\perp \sim r^{-1}$; $T_\parallel \sim r^{-1/2}$; $q \sim r^{-2}$; $\phi_g \sim r^{-1}$; and $\phi_E \sim r^{-1}$. Hence it can be deduced from (23) that at sufficiently large radial distances the energy flux is mainly transported by the heat or conduction term, and

$$\lim_{r\to\infty} (r^2 q) = E_{\infty,p} + E_{\infty,e} = E_\infty \tag{24}$$

where $E_{\infty,p}$ is determined by

$$E_{\infty,p} = \tfrac{1}{4} r_0^2 N_p k T_p \left(\frac{8kT_p}{\pi m_p}\right)^{1/2} \left[2 + \frac{GM(m_p + m_e)}{2kT_p r_0}\right] \tag{25}$$

and a similar expression for $E_{\infty,e}$ (>0). This clearly shows that in the evaporative solar breeze model, E_∞ is different from zero.

In *Chamberlain*'s [1961] hydrodynamic solar breeze model the electron and proton temperatures are assumed to be equal and isotropic ($T = T_\parallel = T_\perp$), and the total heat flux, $q = q_p + q_e$, is given by the classical Chapman-Enskog approximation

$$q = -K_0 T^{5/2}\, dT/dr \tag{26}$$

where $K_0 T^{5/2}$ is the thermal conductivity coefficient of a pure hydrogen plasma [*Spitzer*, 1956].

Chamberlain integrated the hydrodynamic equations with $E_\infty = 0$. This particular solution was chosen to obtain the following two properties: (1) the temperature tends to zero when $r \to \infty$, and (2) the bulk velocity decreases to zero, as in the kinetic solar breeze model. Disregarding in this way all the solutions with a finite bulk velocity at infinity proposed by *Parker* [1958] or more recently by *Durney* [1971, 1972], Chamberlain obtained for $E_\infty = 0$ a hydrodynamic model, which has in some respects a similar asymptotic behavior, as in the evaporative case: $w \sim r^{-1/2}$, $n \sim r^{-3/2}$, and $T \sim r^{-1}$. From this temperature variation and from the classical Chapman-Enskog approximation (26), it follows that $q \sim r^{-9/2}$; i.e., $qr^2 \to 0$ when $r \to \infty$, and hence $E_\infty = 0$. This implies that the subsonic expansion described by *Chamberlain* [1961] becomes adiabatic at large radial distances, or, as stated by *Parker* [1964], that Chamberlain's expanding corona forms a perfect thermal insulator so that there is strictly no heat transfer ($E_\infty = 0$) between the corona, where the temperature is 10^6 °K, and the interplanetary space, where $T \approx 0$.

In Chamberlain's evaporative model, where E_∞ is not zero and $q \sim r^{-2}$, there is, however, some finite heat transport between the corona and the interplanetary space. Therefore, despite the similarity of the radial dependence of the bulk velocity and the density, Chamberlain's kinetic and hydrodynamic solutions are physically not equivalent.

If one follows *Chamberlain*'s [1961] argument that 'it must be possible to reconcile the kinetic and hydrodynamic approaches,' it can be concluded (1) that the integration constant E_∞ in (23) must be different from zero, and (2)

that the classical hydrodynamic approximation fails to give a realistic value of the heat flux when $r \to \infty$.

A quite different demonstration that E_∞ is not zero for the coronal expansion was given by *Parker* [1965*b*]. By evaluating the order of magnitude of the different terms occurring in the left-hand side of (23), Parker showed that near the base of the corona ($r < 2\ R_S$) the leading terms are the (positive) conduction flux and the (negative) flux of gravitational energy. To balance these two contributions and consequently obtain $E_\infty \approx 0$, the coronal temperature or density, or both, must be larger than some critical value calculated by Parker. Since the actual temperatures and number densities in the corona do not satisfy these conditions, it can be concluded from the hydrodynamic point of view that E_∞ must be different from zero, i.e., that Chamberlain's hydrodynamic solution cannot be applied to the coronal expansion [*Parker*, 1965*b*, *c*].

Finally, there is a fundamental weakness in the kinetic solar breeze model: the escape flux of the electrons is 43 times larger than the proton efflux. This is a consequence of the assumption that the electric potential is given by the Pannekoek-Rosseland potential (18). In subsection C4 it has been shown that for such a field the total potential energy is the same for the protons as for the electrons. However, since the thermal speed of the electrons is 43 times larger than for the protons, there will be many more electrons than ions penetrating into the ion exosphere and escaping from the corona. (*Chamberlain* [1960, p. 48] already noted that 'the tendency of the electron gas to escape from the protons will set up a restraining electric field.' The electric field that was adopted, however, 'is just sufficient to reduce the net attractive force on the protons to half the gravitational force' but is not sufficient to avoid the larger thermal escape of the electrons.) To make these fluxes equal it is necessary to increase the potential barrier the electrons have to overcome to escape. The larger outward electric field accelerates then the ions to supersonic velocities.

At large radial distances, the kinetic models presented by the present authors have an asymptotic behavior more or less comparable with the supersonic hydrodynamic models; i.e., $w \to w_\infty$; $n \sim r^{-2}$; $p \sim r^{-2}$; $T_\parallel \to$ const; $T_\perp \sim r^{-2}$; $q \sim r^{-2}$; and $E_\infty \neq 0$ [*Lemaire and Scherer*, 1972*c*]. The energy is carried at great distances by the protons as kinetic energy and enthalpy but also by the heat flux mainly due to the electron component.

Although it is difficult to compare the kinetic solutions (which are of the two-fluid type) to the inviscid conductive one-fluid models set up by *Parker* [1964, 1965*b*], by *Whang and Chang* [1965], and by *Durney* [1971, 1972], it is worthwhile to note that the kinetic models are more 'comparable' with Parker's solution than with the other two. Indeed, in Parker's models the asymptotic behavior is given by $T \sim r^{-2/7}$ and $q \sim r^{-2}$, and it can be deduced from (23) that 'the energy is carried at great distances not only by the particles as kinetic energy but also by thermal conduction as heat.' In Durney's models, on the contrary, the asymptotic behavior is given by $T \sim r^{-4/3}$ and $q \sim r^{-17/3}$, and 'the flow is essentially adiabatic at sufficiently large r, the outward energy flux being primarily kinetic.' On the other hand, in Whang and Chang's model the asymptotic behavior is given by $T \sim r^{-2/5}$ and $q \sim r^{-12/5}$, and the flow is again adiabatic

for $r \rightarrow \infty$ and 'energy is primarily carried outward by the particles as kinetic energy.' A detailed discussion of the asymptotic behavior of these hydrodynamic models is given by *Roberts and Soward* [1972, p. 189].

7. *Kinetic versus Chew-Goldberger-Low Hydromagnetic Models*

Since in the hydrodynamic approach it is assumed that $T_{\parallel} = T_{\perp}$ and that q is given by (26), the temperature variations cannot be compared with those predicted in the kinetic model. The asymptotic behavior of the proton temperatures in the kinetic model are $T_p^{\parallel} \rightarrow$ const, and $T_p^{\perp} \sim r^{-2}$ at large heliocentric distances [*Lemaire and Scherer,* 1972*c*]. This behavior is in compliance with the results obtained from the CGL hydromagnetic approximation when the magnetic field is radial and when the divergence of the heat flux q becomes vanishingly small.

The kinetic and semikinetic models support a much easier comparison with the CGL hydrodymagnetic solar wind models than with the hydrodynamic ones. As shown in subsection B1, the CGL approximations used by *Whang* [1971*b*, 1972], *Hollweg* [1971], and *Leer and Axford* [1972] are fundamentally different from the classical hydrodynamic approximations. By using the CGL double-adiabatic relations for the parallel and perpendicular pressures or temperatures, *Leer and Holzer* [1972] calculated a collisionless solar wind model with a spiral magnetic field and compared their results with those obtained in the semikinetic model of *Chen et al.* [1972] for the same boundary conditions at 20 R_S. The agreement is very satisfactory and proves that both approaches are consistent with each other. It does not imply, however, as quoted by these authors, that the usual hydrodynamic approaches provide a valid description of the collisionless solar wind.

From the discussion in subsection E6 it can be seen that Parker's hydrodynamic solutions and the kinetic solutions give more or less comparable distributions for the density and bulk velocity in the collisionless region, where the mfp is larger than the scale height and where the expansion velocity is supersonic. This may, however, appear to be paradoxical in view of the fact that the classical hydrodynamic approximations were established in the small mfp limit [see *Chapman and Cowling,* 1970]. The reason is that in a supersonic flow regime the bulk velocity distribution (and consequently the density distribution) is not strongly dependent on the partial pressure gradient term in the equation of motion (22). Indeed, when w is much larger than the velocity of sound, the leading terms of this equation are the inertial $nmw\, dw/dr$ and the gravitational $nmGM/r^2$ forces. Therefore even an incorrect expression or an unsatisfactory approximation for the temperature, the pressure tensor, and the heat flux does not drastically change the distribution of $w(r)$ and $n(r)$. The temperatures and higher-order moments, on the contrary, are essentially dependent on the type of approximation made. This conclusion is reinforced in the two-fluid models where the electron temperature is larger than the proton temperature.

On the other hand, when the flow is subsonic (e.g., in Chamberlain's hydrodynamic solar breeze model), the approximation used to determine the pressure tensor components and the heat flux can greatly influence the results.

F. CONCLUSIONS

The solar and polar wind theories have followed quite the same evolution. Starting with hydrodynamic models of increasing complexity and sophistication, it is now accepted that this type of approximation is appropriate in the collision-dominated regions, but should be replaced by different treatments in the collisionless part of the interplanetary medium and of the upper ionosphere. In these regions a CGL hydromagnetic or a kinetic approach can be applied.

Although in the hydrodynamic treatments the zero-pressure boundary condition at infinity is generally used to select a critical supersonic solution, the pressure tensor components in the kinetic formulation are found to be zero at infinity as a consequence of the physical assumption that there are no particles coming from infinity.

The different controversies that occurred during the historical development seem now to be resolved, and the kinetic theory, disregarded for about ten years after Chamberlain's attempt, has recovered a proper place. Indeed, from comparison with the observations, the kinetic formulation predicts many features of the solar and polar winds, despite the inherent limitations.

It is not excluded that improved versions of the kinetic theory described in section C could be formulated that would take into account the scattering processes required to reduce the pressure or temperature anisotropies found in pure collisionless models.

Another new and promising avenue is to consider time-varying kinetic models, since the actual solar wind as well as the polar wind (especially in the winter hemisphere) are found to be strongly time dependent.

An advantage of the kinetic models is obviously that it makes it possible to take into account, in addition to the thermal electrons and ions, different suprathermal particles and field-aligned currents. This is especially useful in polar wind and auroral ion exosphere models. Furthermore, if the corona is to be considered as a collection of streamers, the kinetic theory is also a rather well-suited formulation to model the solar wind.

REFERENCES

Alfvén, H., and C.-G. Fälthammar, *Cosmical Electrodynamics*, 228 pp., Oxford at the Clarendon Press, London, 1963.

Allen, C. W., *Astrophysical Quantities*, 291 pp., Athlone, London, 1963.

Axford, W. I., Observations of the interplanetary plasma, *Space Sci. Rev., 8*, 331–365, 1968*a*.

Axford, W. I., The polar wind and the terrestrial helium budget, *J. Geophys. Res., 73*, 6855–6859, 1968*b*.

Banks, P. M., Dynamical behavior of the polar topside ionosphere, paper presented at NATO Advanced Study Institute on Magnetosphere-Ionosphere Interactions, Espedalen, Norway, 1971.

Banks, P. M., and T. E. Holzer, The polar wind, *J. Geophys. Res., 73*, 6846–6854, 1968.

Banks, P. M., and T. E. Holzer, Reply, *J. Geophys. Res., 74*, 3734–3739, 1969*a*.

Banks, P. M., and T. E. Holzer, Features of plasma transport in the upper atmosphere, *J. Geophys. Res., 74*, 6304–6316, 1969*b*.

Banks, P. M., and T. E. Holzer, High-latitude plasma transport: The polar wind, *J. Geophys. Res., 74*, 6317–6332, 1969*c*.

Barnes, A., R. E. Hartle, and J. H. Bredekamp, On the energy transport in stellar winds, *Astrophys. J., 166,* L53–L58, 1971.

Bauer, S. J., The constitution of the topside ionosphere, in *Electron Density Profiles in Ionosphere and Exosphere,* edited by J. Frihagen, pp. 270–280, North-Holland, Amsterdam, 1966.

Blackwell, D. E., A study of the outer solar corona from a high altitude aircraft at eclipse of 1954 June 30, *Mon. Notic. Roy. Astron. Soc., 116,* 56–58, 1956.

Brandt, J. C., *Introduction to the Solar Wind,* 199 pp., W. H. Freeman, San Francisco, Calif., 1970.

Brandt, J. C., and J. P. Cassinelli, Interplanetary gas, 11, An exospheric model of the solar wind, *Icarus, 5,* 47–63, 1966.

Burlaga, L. F., and K. W. Ogilvie, Heating of the solar wind, *Astrophys. J., 159,* 659–670, 1970.

Chamberlain, J. W., Interplanetary gas, 2, Expansion of a model solar corona, *Astrophys. J., 131,* 47–56, 1960.

Chamberlain, J. W., Interplanetary gas, 3, A hydrodynamic model of the corona, *Astrophys. J., 133,* 675–687, 1961.

Chamberlain, J. W., On the existence of slow solutions in coronal hydrodynamics, *Astrophys. J., 141,* 320–322, 1965.

Chapman, S., Notes on the solar corona and the terrestrial ionosphere, *Smithson. Contrib. Astrophys., 2,* 1–12, 1957.

Chapman, S., The solar corona and the interplanetary gas, in *Space Astrophys.,* edited by W. Liller, pp. 133–149, McGraw-Hill, New York, 1961.

Chapman, S., and T. G. Cowling, *The Mathematical Theory of Nonuniform Gases,* 423 pp., Cambridge University Press, New York, 1970.

Chen, W. M., C. S. Lai, H. E. Lin, and W. C. Lin, Collisionless solar wind in the spiral magnetic field, *J. Geophys. Res., 77,* 1–11, 1972.

Chew, G. F., M. L. Goldberger, and F. E. Low, The Boltzmann equation and the one-fluid hydromagnetic equations in the absence of particle collisions, *Proc. Roy. Soc. London, Ser. A, 236,* 112–118, 1956.

Cuperman, S., and A. Harten, The solution of one-fluid equations with modified thermal conductivity for the solar wind, *Cosmic Electrodyn., 1,* 205–217, 1970*a*.

Cuperman, S., and A. Harten, Noncollisional coupling between the electron and the proton components in the two-fluid model of the solar wind, *Astrophys. J., 162,* 315–326, 1970*b*.

Cuperman, S., and A. Harten, The electron temperature in the two-component solar wind, *Astrophys. J., 163,* 383–392, 1971.

Dahlberg, E., Viscous model of solar wind flow, *J. Geophys. Res., 75,* 6312–6317, 1970.

Dessler, A. J., Solar wind and interplanetary magnetic field, *Rev. Geophys. Space Phys., 5,* 1–41, 1967.

Dessler, A. J., and P. A. Cloutier, Discussion of letter by Peter M. Banks and Thomas E. Holzer, 'The polar wind,' *J. Geophys. Res., 74,* 3730–3733, 1969.

Dessler, A. J., and F. C. Michel, Plasma in the geomagnetic tail, *J. Geophys. Res., 71,* 1421–1426, 1966.

Donahue, T. M., Polar ion flow: Wind or breeze?, *Rev. Geophys. Space Phys., 9,* 1–9, 1971.

Dungey, J. W., Interplanetary magnetic field and the auroral zones, *Phys. Rev. Lett., 6,* 47–48, 1961.

Dungey, J. W., The theory of the quiet magnetosphere, in *Solar-Terrestrial Physics,* edited by J. W. King and W. S. Newman, pp. 91–106, Academic, London, 1967.

Durney, B. R., A new type of supersonic solution for the inviscid equations of the solar wind, *Astrophys. J., 166,* 669–673, 1971.

Durney, B. R., Solar-wind properties at the earth as predicted by one-fluid models, *J. Geophys. Res., 77,* 4042–4051, 1972.

Eisler, T., Asymptotic solutions of the viscous solar wind equations, *Solar Phys., 7,* 49–53, 1969.

Eviatar, A., and M. Schulz, Ion-temperature anisotropies and the structure of the solar wind, *Planet. Space Sci., 18,* 321–332, 1970.

Forslund, D. W., Instabilities associated with heat conduction in the solar wind and their consequences, *J. Geophys. Res., 75,* 17–28, 1970.

Griffel, D. H., and L. Davis, The anisotropy of the solar wind, *Planet. Space Sci., 17,* 1009–1020, 1969.

Hartle, R. E., and A. Barnes, Nonthermal heating in a two-fluid solar wind model, *J. Geophys. Res., 75,* 6915–6931, 1970.

Hartle, R. E., and P. A. Sturrock, Two-fluid model of the solar wind, *Astrophys. J., 151,* 1155–1170, 1968.

Hoffman, J. H., Ion composition measurements in the polar region from the Explorer 31 satellite, *EOS Trans. AGU, 49,* 253, 1968.

Hoffman, J. H., Studies of the composition of the ionosphere with a magnetic deflection mass spectrometer, *Int. J. Mass Spectrom. Ion Phys., 4,* 315–322, 1970.

Hoffman, J. H., Polar wind measurements, *EOS Trans. AGU, 52,* 301, 1971.

Hollweg, J. V., Collisionless solar wind, 1, Constant electron temperature, *J. Geophys. Res., 75,* 2403–2418, 1970.

Hollweg, J. V., Collisionless solar wind, 2, Variable electron temperature, *J. Geophys. Res., 76,* 7491–7502, 1971.

Hollweg, J. V., and H. J. Völk, New plasma instabilities in the solar wind, *J. Geophys. Res., 75,* 5297–5309, 1970.

Holt, E. H., and R. E. Haskell, *Foundations of Plasma Dynamics,* 510 pp., Macmillan, New York, 1965.

Holzer, T. E., and W. I. Axford, The theory of stellar winds and related flows, *Ann. Rev. Astron. Astrophys., 8,* 31–60, 1970.

Holzer, T. E., J. A. Fedder, and P. M. Banks, A comparison of kinetic and hydrodynamic models of an expanding ion-exosphere, *J. Geophys. Res., 76,* 2453–2468, 1971.

Hundhausen, A. J., Direct observations of solar-wind particles, *Space Sci. Rev., 8,* 690–749, 1968.

Hundhausen, A. J., Composition and dynamics of the solar wind plasma, *Rev. Geophys. Space Phys., 8,* 729–811, 1970.

Hundhausen, A. J., Composition and dynamics of the solar wind plasma, in *Solar-Terrestrial Physics/1970,* part 2, edited by E. R. Dyer, pp. 1–31, D. Reidel, Dordrecht, Netherlands, 1972*a*.

Hundhausen, A. J., *Coronal Expansion and Solar Wind,* 238 pp., Springer, Berlin, 1972*b*.

Hundhausen, A. J., S. J. Bame, J. R. Asbridge, and S. J. Sydoriak, Solar wind proton properties: Vela 3 observations from July 1965 to June 1967, *J. Geophys. Res., 75,* 4643–4657, 1970.

Jacchia, L. G., Static diffusion models of the upper atmosphere with empirical temperature profiles, *Smithson. Contrib. Astrophys., 8,* 215–257, 1965.

Jeans, J. H., *The Dynamical Theory of Gases,* 444 pp., Dover, New York, 1954.

Jensen, E., Mass losses through evaporation from a completely ionized atmosphere with applications to the solar corona, *Astrophys. Norv., 8,* 99–126, 1963.

Jockers, K., Solar wind models based on exospheric theory, *Astron. Astrophys., 6,* 219–239, 1970.

Jones, J. E., Free paths in a non-uniform rarefied gas with an application to the escape of molecules from isothermal atmospheres, *Trans. Cambridge Phil. Soc., 22,* 535–556, 1923.

Kennel, C. F., and F. L. Scarf, Thermal anisotropies and electromagnetic instabilities in the solar wind, *J. Geophys. Res., 73,* 6149–6165, 1968.

Konyukov, M. V., Plasma outflow from the sun with viscosity playing a significant role, *Geomagn. Aeron., 9,* 1–6, 1969.

Koons, H. C., D. A. McPherson, and M. Schulz, Ion-wave instabilities at VLF in the polar wind, *J. Geophys. Res., 76,* 6122–6135, 1971.

Leer, E., and W. I. Axford, A two-fluid solar wind model with anisotropic proton temperature, *Solar Phys., 23,* 238–250, 1972.

Leer, E., and T. E. Holzer, Collisionless solar wind protons: A comparison of kinetic and hydrodynamic descriptions, *J. Geophys. Res., 77,* 4035–4051, 1972.

Lemaire, J., The relations between the temperatures and velocity in kinetic models of the solar wind, paper presented at 1st European Earth and Planetary Physics Colloquium, Reading, England, 1971.

Lemaire, J., O^+, H^+ and He^+ ion distributions in a new polar wind model, *J. Atmos. Terr. Phys., 34,* 1647–1658, 1972*a*.

Lemaire, J., Effect of escaping photoelectrons in a polar exospheric model, *Space Res., 12,* 1414–1416, 1972*b*.

Lemaire, J., and M. Scherer, Le champ électrique de polarisation dans l'exosphère ionique polaire, *C.R.H. Acad. Sci., Ser. B, 269,* 666–669, 1969.

Lemaire, J., and M. Scherer, Model of the polar ion-exosphere, *Planet. Space Sci., 18,* 103–120, 1970.

Lemaire, J., and M. Scherer, Simple model for an ion-exosphere in an open magnetic field, *Phys. Fluids, 14,* 1683–1694, 1971*a*.

Lemaire, J., and M. Scherer, Kinetic models of the solar wind, *J. Geophys. Res., 76,* 7479–7490, 1971*b*.

Lemaire, J., and M. Scherer, Ion-exosphere with asymmetric velocity distribution, *Phys. Fluids, 15,* 760–766, 1972*a*.

Lemaire, J., and M. Scherer, The effect of photoelectrons on kinetic polar wind models, *Bull. Cl. Sci. Acad. Roy. Belg., 58,* 502–512, 1972*b*.

Lemaire, J., and M. Scherer, Comportements asymptotiques d'un modèle cinétique du vent solaire, *Bull. Cl. Sci. Acad. Roy. Belg., 58,* 1112–1134, 1972*c*.

Lemaire, J., and M. Scherer, Plasma sheet particle precipitation: A kinetic model, *Planet. Space Sci., 21,* 281–289, 1973.

Macmahon, A., Finite gyro-radius corrections to the hydromagnetic equations for a Vlasov plasma, *Phys. Fluids, 8,* 1840–1845, 1965.

Mange, P., The exosphere and geocorona, in *Solar-Terrestrial Physics/1970,* Part 4, edited by E. R. Dyer, pp. 68–86, D. Reidel, Dordrecht, Netherlands, 1972.

Marubashi, K., Escape of the polar-ionospheric plasma into the magnetospheric tail, *Rep. Ionos. Space Res. Jap., 24,* 322–346, 1970*a*.

Marubashi, K., Structure of topside ionosphere in high latitudes, *J. Radiat. Res., 17,* 335–416, 1970*b*.

Michard, R., Densités électroniques dans la couronne externe du 25 Février 1952, *Ann. Astrophys., 17,* 429–442, 1954.

Montgomery, D. C., and D. A. Tidman, Plasma kinetic theory, 293 pp., McGraw-Hill, New York, 1964.

Montgomery, M. D., S. J. Bame, and A. J. Hundhausen, Solar wind electrons: Vela 4 measurements, *J. Geophys. Res., 73,* 4999–5003, 1968.

Ness, N. F., The earth's magnetic tail, *J. Geophys. Res., 70,* 2989–3005, 1965.

Ness, N. F., Observed properties of the interplanetary plasma, *Annu. Rev. Astron. Astrophys., 6,* 79–114, 1968.

Nicolet, M., Helium, an important constituent in the lower exosphere, *J. Geophys. Res., 66,* 2263–2264, 1961.

Nishida, A., Formation of plasmapause, or magnetospheric plasma knee, by the combined action of magnetospheric convection and plasma escape from the tail, *J. Geophys. Res., 71,* 5669–5679, 1966.

Noble, L. M., and F. L. Scarf, Conductive heating of the solar wind, 1, *Astrophys. J., 138,* 1169–1181, 1963.

Pannekoek, A., Ionization in stellar atmospheres, *Bull. Astron. Inst. Neth., 1,* 107–118, 1922.

Parker, E. N., Dynamics of the interplanetary gas and magnetic fields, *Astrophys. J., 128,* 664–676, 1958.

Parker, E. N., *Interplanetary Dynamical Processes,* 272 pp., Interscience, New York, 1963.

Parker, E. N., Dynamical properties of stellar coronas and stellar winds, 2, Integration of the heat-flow equation, *Astrophys. J., 139,* 93–122, 1964.

Parker, E. N., Dynamical theory of the solar wind, *Space Sci. Rev., 4,* 666–708, 1965*a*.

Parker, E. N., Dynamical properties of stellar coronas and stellar winds, 4, The separate existence of subsonic and supersonic solutions, *Astrophys. J., 141,* 1463–1478, 1965*b*.

Parker, E. N., On the existence of slow solutions in coronal hydrodynamics, *Astrophys. J., 141,* 322–324, 1965*c*.

Parker, E. N., The dynamical theory of gases and fields in the interplanetary space, in *Solar-Terrestrial Physics,* edited by J. W. King and W. S. Newman, pp. 45–55, Academic, New York, 1967.

Parker, E. N., Theoretical studies of the solar wind phenomenon, *Space Sci. Rev., 9,* 325–360, 1969.

Parker, E. N., Recent developments in theory of solar wind, *Rev. Geophys. Space Phys., 9,* 825–835, 1971.

Pikel'ner, S. B., On the theory of the solar corona (in Russian), *Izv. Krym. Astrofiz. Observ., 5,* 34, 1950.

Pottasch, S. R., Use of the equation of hydrostatic equilibrium in determining the temperature distribution in the outer solar atmosphere, *Astrophys. J., 131,* 68–74, 1960.

Roberts, P. H., and A. M. Soward, Stellar winds and breezes, *Proc. Roy. Soc. London, Ser. A, 328,* 185–215, 1972.

Rosseland, S., Electrical state of a star, *Mon. Notic. Roy. Astron. Soc., 84,* 720–728, 1924.

Scarf, F. L., Microscopic structure of the solar wind, *Space Sci. Rev., 11,* 234–270, 1970.

Scarf, F. L., and L. M. Noble, Conductive heating of the solar wind, 2, The inner corona, *Astrophys. J., 141,* 1479–1491, 1965.

Scarf, F. L., J. H. Wolfe, and R. W. Silva, A plasma instability associated with thermal anisotropies in the solar wind, *J. Geophys. Res., 72,* 993–1005, 1967.

Schulz, M., and A. Eviatar, Electron-temperature asymmetry and the structure of the solar wind, *Cosmic Electrodyn., 2,* 402–422, 1972.

Sen, H. K., The electric field in the solar coronal exosphere and the solar wind, *J. Franklin Inst., 287,* 451–456, 1969.

Serbu, G. P., Explorer 35 observations of solar wind electron density, temperature, and anisotropy, *J. Geophys. Res., 77,* 1703–1712, 1972.

Spitzer, L., Jr., *Physics of Fully Ionized Gases,* 105 pp., Interscience, New York, 1956.

Stratton, J. A., *Electromagnetic Theory,* 615 pp., McGraw-Hill, New York, 1941.

Sturrock, P. A., and R. E. Hartle, Two-fluid model of the solar wind, *Phys. Rev. Lett., 16,* 628–631, 1966.

Tan, M., and B. Abraham-Shrauner, Solar wind for a magnetized plasma with tensor plasma pressure, *Cosmic Electrodyn., 3,* 71–80, 1972.

Taylor, H. A., Jr., H. C. Brinton, M. W. Pharo III, and N. K. Rahman, Thermal ions in the exosphere; Evidence of solar and geomagnetic control, *J. Geophys. Res., 73,* 5521–5533, 1968.

Urch, I. H., A model of the magnetized solar wind, *Solar Phys., 10,* 219–228, 1969.

van de Hulst, H. C., The chromosphere and corona, in *The Sun,* edited by G. P. Kuiper, pp. 307–321, University of Chicago Press, Chicago, Ill., 1953.

Weber, E. J., Unique solutions of solar winds models with thermal conductivity, *Solar Phys., 14,* 480–488, 1970.

Weber, E. J., and L. Davis, Jr., The angular momentum of the solar wind, *Astrophys. J., 148,* 217–227, 1967.

Weber, E. J., and L. Davis, Jr., The effect of viscosity and anisotropy in the pressure on the azimuthal motion of the solar wind, *J. Geophys. Res., 75,* 2419–2428, 1970.

Whang, Y. C., Conversion of magnetic-field energy into kinetic energy in the solar wind, *Astrophys. J., 169,* 369–378, 1971*a*.

Whang, Y. C., Higher-moment equations and the distribution function of solar-wind plasma, *J. Geophys. Res., 76,* 7503–7507, 1971*b*.

Whang, Y. C., A solar-wind model including proton thermal anisotropy, *Astrophys. J., 178,* 221–239, 1972.

Whang, Y. C., and C. C. Chang, An inviscid model of the solar wind, *J. Geophys. Res., 70,* 4175–4180, 1965.

Whang, Y. C., C. K. Liu, and C. C. Chang, A viscous model of the solar wind, *Astrophys. J., 145,* 255–269, 1966.

Wilcox, J. M., The interplanetary field: Solar origin and terrestrial effects, *Space Sci. Rev., 8,* 258–358, 1968.

Wolff, C. L., J. C. Brandt, and R. G. Southwick, A two-component model of the quiet solar wind viscosity, magnetic field, and reduced heat conduction, *Astrophys. J., 165,* 181–194, 1971.

(Received November 13, 1972; revised February 5, 1973.)